Materials Science in Semiconductor Processing 92 (2019) 58–72

Contents lists available at ScienceDirect

Materials Science in Semiconductor Processing

journal homepage: www.elsevier.com/locate/mssp

Thermal reflow of polymers for innovative and smart 3D structures: A review

Robert Kirchner[a,b,*], Helmut Schift[b]

[a] Technische Universität Dresden, Institute of Semiconductors and Microsystems, 01062 Dresden, Germany
[b] Paul Scherrer Institute, Laboratory for Micro and Nanotechnology, 5232 Villigen PSI, Switzerland

ARTICLE INFO

Keywords:
Grayscale
Lithography
Visco-elasticity
Softening
Surface tension
Flow
Capillary force

ABSTRACT

This is a topical review on advanced lithographic methods used to create 3D topographies. We start the discussion with the principal capabilities of grayscale electron beam lithography and multi-photon lithography for initial patterning. The innovative structures in this work become only possible by *combining* the initial patterns with methods to reshape them. By this, new functionalities such as aspheric, freeform and ultra-smooth surfaces can be provided. All the covered methods have in common that they exploit a specific material contrast that enables a post-processing and thus a transformation of the initial pattern by polymer reflow into a new surface topography or shape. To enhance the understanding of current reflow methods, we review the history of polymer reflow and discuss its simulation. In-depth examples cover optical and biomimetic applications. Furthermore, we provide new results and new insights into dynamic material changes during thermoplastic reflow. An outlook on emerging 3D MEMS fabrication using thermoplastic polymer reflow for actuation will illuminate the way towards smart, i.e, stimuli responsive 3D structures. This review is mainly meant for applied scientists and engineers.

1. Introduction

In micro- and nanofabrication, thermal reflow generally describes the concept of reshaping initial patterns into new profiles. While the initial structure can be obtained from efficient standard processes, the reshaped and new profile can most often only be obtained with reasonable efforts by reflow. In non-technical applications, reflow is like melting sugar grains into droplets or merging them into a smooth crust of caramelized sugar on a *Crème brulée*. On the technical side, one prominent example is the fabrication of microlenses, i.e., lenses with curved surfaces and some tens of micrometer up to a few millimeters in diameter. Such lenses, often arranged in arrays, are used for beam shaping and illumination [1–3]. Similar to macroscopic lenses with concave and convex shapes, microlenses require both a continuous contour able to redirect light by refraction and a smooth surface with roughness much below the wavelength to be used. This can be achieved by reshaping lithographically obtained initial photoresist structures with box-type contours (i.e., vertical sidewalls) into hemispherical structures (i.e., curved sidewalls) by heating the resist beyond its softening point. Another example for reflow is curved solder bump formation from box-like initial solder volumes [4]. The box-like structures are prepared for example from screen-printing a solder paste. Subsequently, the structures are reshaped at high temperatures, well beyond the melting point of the solder, into perfect hemispheres or balls. Both examples demonstrate the transformation of a typical binary structure (i.e. 2- or 2.5-dimensional) into a more complex structure with 3-dimensional (3D) contours. The transformation is achieved by heating the initial structures into a regime where the material is able to flow. The obtained shape remains preserved once the material is solidified (cooled). The reason for reshaping is the surface tension. It transforms the initial and energetically unfavorable box structures into a drop-like structure with a minimal energy surface. Usually, the complete initial material is homogeneous and behaves isotropic (Fig. 1a homogeneous). In case of photoresist reflow, e.g., a round disk of resist results in a micro-lens shape that is centrosymmetric. In contrast to this, in inhomogeneous materials, i.e., materials where a local difference in the material and thus in the ability of flow at a given temperature is present (Fig. 1a contrast) this will be different. The flow will be inhomogeneous in nature and may result in a variety of shapes not possible with homogeneous material. This review mainly considers initial shapes that are inhomogeneous in material composition, i.e., materials that have a certain contrast in its composition and in consequence in its thermomechanical properties. This contrast can be achieved by different kind of energetic radiation such as ions, x-rays, protons or as in

* Corresponding author.
E-mail address: robert.kirchner@tu-dresden.de (R. Kirchner).

https://doi.org/10.1016/j.mssp.2018.07.032
Received 12 March 2018; Received in revised form 17 July 2018; Accepted 19 July 2018
Available online 13 August 2018
1369-8001/

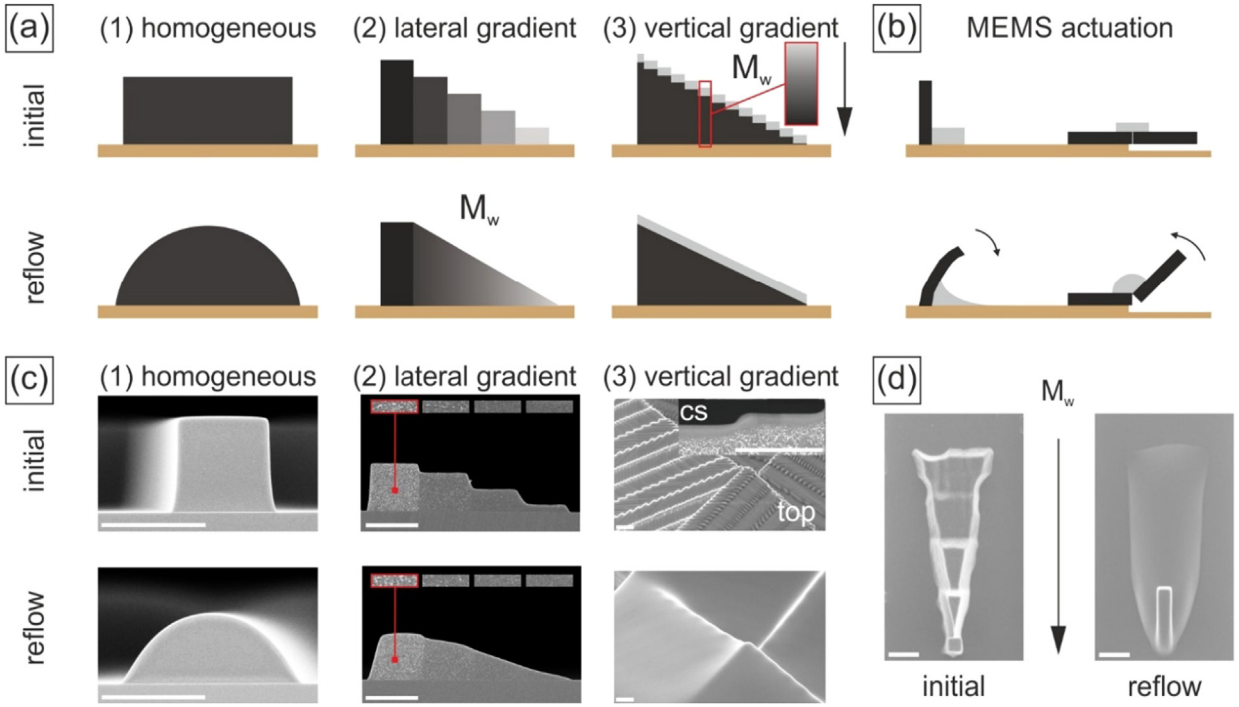

Fig. 1. Overview on main reflow concepts being covered in this review using variations of the material contrast (black: unmodified material, gray: modified material). **(a)** Schematic comparison of three different scenarios: **(1) homogeneous material** (no material contrast) leading to a spherical or cylindrical shape due to reflow of the entire material. **(2) lateral material contrast** (increasing resist modification) being visible in different granularity (insets) after electron beam exposure and enabling asymmetric reflow due to inhomogeneous and graded material properties. **(3) vertical contrast** (unmodified bulk with modified skin) enabling selective reflow in a limited superficial region without effect on the bulk. **(b)** Schematic MEMS actuation using polymer reflow with the two examples *off-axis bending* and *out-of-plane rotation* due to hinges with modified polymer. **(c-d)** Respective experimental results for (a) and (b) showing real structures before (initial) and after reflow. (reprinted in parts with permission © Wiley/AMT) (top: top view and cs: cross-sectional scanning electron micrograph, all scale bars 2 µm).

this topical review by electrons and high-energy photons [5–8].

Grayscale electron beam lithography (GEBL) is key to create almost arbitrary, high-resolution 3D surface topographies – by exposure only and in combination with reflow. The essential part in GEBL is an exposure-induced material contrast [9–15]. This is contrary to binary lithography, where we distinguish only between exposed and non-exposed sections of an extended resist film, resulting in preserved and cleared areas of resist. Grayscale lithography uses a modulated intensity exposure which results in a graded material contrast. While the binary exposure, e.g., in case of positive resist, enables complete removal of the exposed resist, this graded material contrast enables to achieve a dose-dependent removal of the resist height. The height accuracy that is required in discrete stepped profiles for most advanced optical applications can be obtained via advanced consideration of 3D proximity effects, development effects and advanced process optimization [16–22]. There is also photon-based grayscale lithography. It is widely adapted for grayscale photolithography (GPL) by using different exposure methods including half-toning, partially transparent masks or laser direct writing [23–28]. However, most photon-effects are linked to the chemical composition leading to differences in dissolution rates in typical photoresists. There is no significant handle for the thermo-mechanical properties and thus the ability to control reflow by photo-exposure such as in GEBL. An exception are negative tone photoresists like SU-8 or photo-sensitized PMMA where the exposure increases cross-linking and thus reduces the ability to reflow or being reshaped by other methods [29–32]. In contrast, patterning linear polymers such as poly(methyl methacrylate) (PMMA) by photons, e.g., in grayscale extreme ultraviolet (EUV) lithography [33] *has* an effect the thermo-mechanical properties.

To extend the feature diversity and to obtain new patterns, polymer reflow *in combination* with grayscale methods offers a versatile patterning toolbox [34–36]. Reflow by thermal annealing is used also in different other technologies to reach structural perfection. For example, simple reflow of thermoplastic waveguides by gentle heating enabled a much better transmission due to less scattering losses due to lower surface roughness [37]. High-temperature reflow is also available for inorganic materials to reduce waveguide losses [38] and to produce high-Q toroid laser resonators [39,40]. Also spun-on films over topography can be smoothed by reflow [41]. It should be noted that, in contrast to the waveguide smoothening above, resist sidewall smoothening was also discussed to be a consequence of outgassing [42] and maybe not only of reflow. Key to the roughness reduction by reflow is the ability of a material to relocate or rearrange at elevated temperatures. By heating, the material becomes softer than at room temperature and is able to follow faster surface tension forces. This was also exploited for guided pattern formation using temperature induced instabilities in thin films [43,44]. In block-copolymer directed self-assembly (DSA), thermal annealing is used to enhance the mobility of the polymer chain segments to allow for an energy-optimized rearrangement, i.e., phase-separation [45].

In all of the mentioned applications, total systems energy optimization plays a key role. The total systems energy is in most cases defined by surface energy and entropy. Except for the DSA, the material usually is of a homogeneous composition. For DSA, two types of polymers co-assembled in one polymer chain form a heterogeneous system. In the approaches reviewed here, a homogeneous material with linear polymer chains of defined molecular weight $M_{w,homo}$ is first modified into a heterogeneous material with segments of the initial linear polymer chain with reduced molecular weight $M_{w,hetero} < M_{w,homo}$. The material remains the same but has different properties. There are already numerous papers on the above mentioned techniques. This review will remain with the reflow using lateral and vertical material contrast (cf. Fig. 1a,c) generated by high-energy particle impact of electrons and photons on linear thermoplastic materials such as PMMA.

A short outlook on applications of reflow of polymers for microsystems (MEMS) will be given as well (cf. Fig. 1b,d).

The remaining paper will be organized as following. We first discuss in Section 2 how to create a proper localized material contrast in a homogeneous material that enables a temperature selective reflow. In Section 3 the temperature selective reflow is compared to the classical reflow of microlenses. Furthermore, different simulation concepts of reflow are emphasized to enhance the understanding of the basic physical effects playing a role in polymer reflow. Finally. Section 4 gives several examples on how to make use of temperature selective reflow for various applications in a tutorial fashion.

2. Material contrast: from exposure to viscous flow

2.1. From molecular weight M_w to glass transition temperature T_g

Basically, the glass transition temperature T_g of a thermoplastic material defines the transition region between an rigid and a rubbery polymer state. The T_g strongly depends on the molecular weight especially below a certain threshold known as critical molecular weight M_c [46]. Typically, M_n and M_w are used to describe the molecular weight of macromolecules like polymers. While the number averaged value M_n is required for most physicochemical explanations, the weight averaged value M_w is more of applied engineering use. Both values are related via the polydispersity (cf. Section 2.2). The M_c is a material specific number describing a threshold in polymer chain length and thus number of entanglements, below and above which T_g and also viscosity scales differently with the molecular weight. Thus, the M_n (and thus M_w) can be used as a means to control the T_g, with an especially strong effect once the M_n drops below the M_c. The M_w of linear polymers can be changed by modifying the average chain length. Either crosslinking or bond cleavage can be used for this. To reduce the M_w and thus the T_g, a bond cleavage is required. This is usually achieved by high-energy radiation impact on the polymer [47,48]. Therefore: As long as the polymer chain fragments are large enough that they do not become volatile, and main chain scission is a major effect of M_w reduction, they will exhibit the same chemical behavior as the initial long chain and will only differ in terms of M_w, resulting in a decrease of T_g and thus the corresponding viscosity η at a specific process temperature T. Typical radiation probes include ions, protons, electrons, X-rays and photons produced from different sources [48,49]. Depending on the probe, the M_w reduction follows different routes and has different efficiencies [49]. Based on the ratio of main chain scissions to the number of changed ester groups as well as to number of unsaturated bonds being created, high energy radiation is much more efficient in material modification then for example deep UV radiation of PMMA. Based on this, the efficiency is high for X-rays (~ 0.8–1.8 keV), protons (~ 300 keV) and electrons (~ 25 keV) and much lower for deep UV (4–6 eV) [49]. High-energy electrons (100 keV) are considered to be less efficient than 25 keV electrons but are still more efficient than deep UV radiation. 13.5 nm EUV (~ 92 eV) and 172 nm vacuum UV (~ 7 eV) photon radiation was found to be more efficient than 100 keV electrons, where EUV is more efficient than VUV in terms of energy required to obtain the same material effect. Fallica et al. [50] recently introduced a concept of chemical sensitivity which describes the volume of cleared resist per absorbed EUV photon. This model is summing up all effects following the absorption event of photons and is, even though developed for EUV lithography, quite appealing to be used to characterize the effect of different kind of radiation on the M_w of solvent soluble materials in general. The interpretation in this review context is: the higher the chemical sensitivity is, the more material volume is altered in its properties.

2.2. Role of polymer dispersity

The polydispersity of linear thermoplastics describes the distribution of the molecular masses based on the ratio of weight M_w and number averaged M_n molecular weights. While there is a clear relation for the absolute value of the molecular weight and the T_g, it is not so clear for the influence of polydispersity. Larger molecular weights will result in a larger T_g and thus requires a higher temperature to initiate reflow. It was recently reported that the polydispersity has little influence on the T_g [51]. Experiments with electron beam exposure showed that the initially large polydispersity of the commercial resist was not significantly altered by typical exposure doses [36]. This demonstrates that in practical situations the T_g is rather controlled via the absolute value of the molecular weight rather than via the polydispersity.

2.3. Creating T_g contrast in lateral and vertical direction

The essential task of lithography is creating material contrast in lateral (in-plane) direction by design. By scanning for example high-energy electrons, different regions of M_w and thus T_g can be obtained with high spatial resolution and in relative thick materials. Due to the large acceleration voltages, the material is exposed from its surface down to its bottom without significant loss due to absorption. This is important for GEBL. By applying different doses of exposure to different lateral sections of the resist, either by scanning of a focused beam or by masking a flood exposure, different sections of M_w are obtained in lateral direction. The dose can be seen as an equivalent to the number of electrons able to cause chain scissions. While typically only the difference in M_w and thus solvent removal rate of the resist is used in binary lithography, the M_w differences also result in a strong local contrast in reflow behavior [36]. These patterns are almost homogeneously in its depth distribution of the M_w but can be laterally varied with very high resolution (high resolution = steep lateral contrast). This is due to the high electron acceleration energy and the minimum forward and backward scattering. Exploiting GEBL to write grayscale initial patterns for reflow serves to purposes: (i) geometric shape definition and (ii) material property definition. Both aspects are linked to each other via the used developer and developing conditions providing large freedom in process design. To be efficient, a minimum number of grayscale levels is used to prescribe the required shape, an optical lens for example (Figs. 10, 11). The same concept was also used to create ultra-smooth and varyingly tapered funnel structures as molds for replication of biomimetic structures meant to reduce solid-state friction (Fig. 15).

To obtain a vertical contrast in a film, i.e., modifying the molecular weight in a limited depth to which reflow can be confined later on, a selective process is required contrary to the afore mentioned lateral contrast. This can be done by photons which wavelength together with the materials linear absorption coefficient defines the maximal photon penetration depth. This in turn defines the maximum depth of the Lambert-Beer type exponentially decaying material modification. For example EUV (13.5 nm) or vacuum UV (172 nm) photons both have roughly a linear absorption coefficient of 5 μm^{-1} [8] in PMMA. In 500 nm depth, this will result in an intensity reduction to less than 10% of the surface intensity. One can thus assume the maximum modification depth to be in the range of 500 nm in PMMA. This can be used to generate ultra-smooth optical surfaces from initially microscopically rough micro-lenses in combination with reflow [8]. Thereby, the lens fabrication process can be significantly optimized for throughput but at the same time make use of new but partially slow lithography techniques such as multi-photon lithography [52]. Such smoothening might be even interesting for 3D printed parts designed for use in the THz regime [53] or for microfluidic applications.

2.4. Contrast in viscosity η

Not the glass transition temperature T_g, but the viscosity η at a given temperature is the major property needed to describe M_w selective

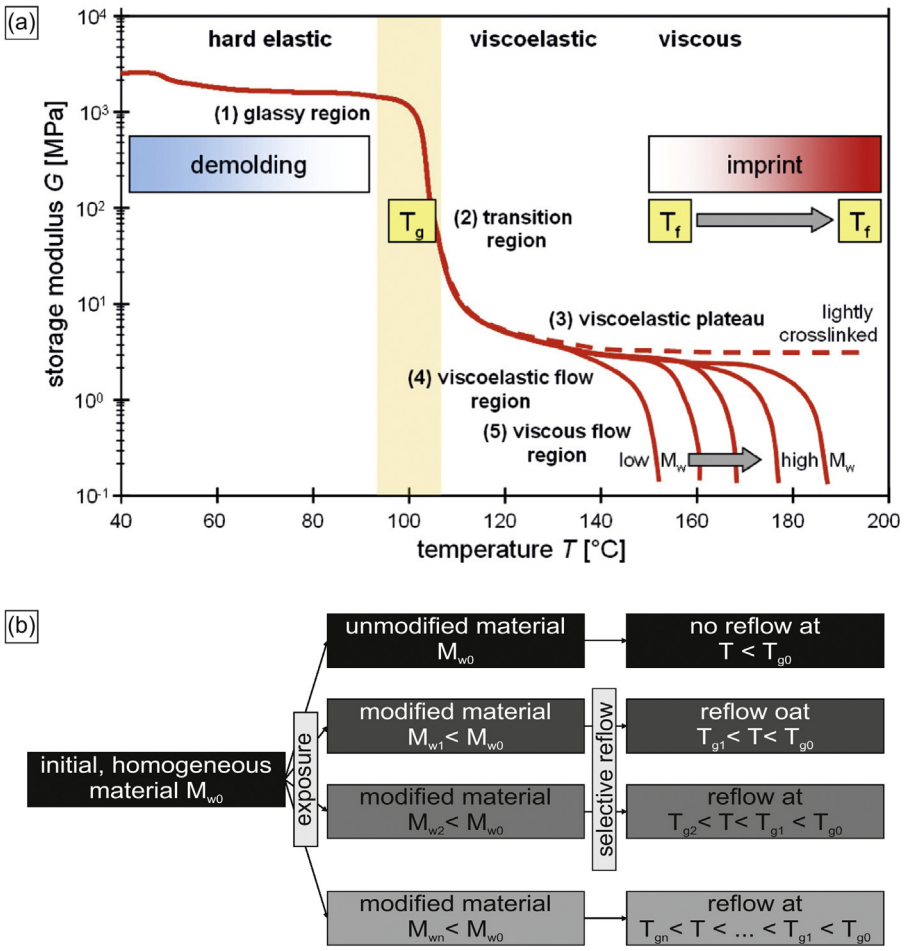

Fig. 2. (a) Mechanical properties of polymers dependent on temperature, molecular weight, and crosslinking (Ref [58]., modified from Ref [59]. Schematic for a polymer with a T_g around 100 °C for normal process conditions. (reprinted with permission [58] (c) AVS/JVSTB) **(b)** Schematic on selective thermal reflow: typical reflow temperatures are $T_g \ll T_{reflow}$. However, due to the fact that T_g is defined as a region rather than a sharp transition, for localized selective reflow $T_{gn} < T_{reflow} < T_{g0}$, reflow temperature and time have to be chosen adequately so that differences in viscosity become significant between modified and non-modified material.

thermal flow. However, viscosity is difficult to measure on a local scale. Often these values are determined using a double-plate shear instrument, which – similarly to T_g measurements with differential scanning calorimetry (DSC) – requires a considerable amount of material. In previous experiments, this was done by spin-coating a PMMA film on a silicon wafer and detaching the film from the surface by delamination. Using different homogeneous exposure doses over the entire surface, films of different M_w could be obtained [36]. However, even then, the measured viscosity may be different from that of a thin supported film with inhomogeneous material distribution or surface pattern. Localized measurement of η using scanning probes have been examined, however, the temperature range needed for reflow, even if at temperatures below the original T_g, are often not acceptable for typical scanning force microscopes and indenters. Furthermore, the influence of the substrate and shear effects cannot be easily excluded for the thin films typically used for grayscale lithography. One possibility to estimate viscosities is the fit of simulation models to real experimental results and an inverse simulation parameter extraction (cf. Section 3.4)

3. Reflow

Thermal reflow is defined here as the material relocation or displacement above a certain threshold temperature T_{th} driven by surface tension. This surface tension flow requires a free surface and is thus fundamentally different from squeezed flow situations such as in embossing, nanoimprint lithography (NIL) or injection molding and also differs from capillary flow in microfluidics or related methods. Once the reflow material becomes viscous enough, it loses its constraints: polymer chains can move freely within geometrical boundaries and are governed by cohesion; surfaces can adjust to geometrical boundaries defined by surface energy and material properties such as adhesion and wettability at interfaces. After cooling, the polymer is solidified in a shape which is either at the equilibrium of total systems energy or in an intermediate state. There is an extensive list of literature on the reflow of photoresist materials for microlens manufacturing and this work will only summarize the consensus extracted from the respective literature to compare it with the reflow process of thermoplastic materials such as PMMA used in this work. In both methods, the energetic optimization of the shape is driven by surface tension forces that are able to reshape the initial pattern once the mobility of the polymer chains are high enough to allow for the required material displacement. Thus, two components are required for reflow: (i) sufficiently high surface tension and (ii) sufficiently low viscosity (or high mobility) at a given temperature to enable material relocation in a certain time interval.

3.1. Classical reflow process: patterned photoresist

Compared to the reflow of linear thermoplastic materials, the reflow of photoresist materials involves complex material processes. Photoresists are used for reflow because they are optimized for photolithographic patterning and pattern transfer including resist demands such as high optical sensitivity, high resolution, high chemical and etch stability as well as good adhesion to the substrate. Photoresists *are not* optimized for reflow and involve certain aspects that are suboptimal for reflow. For example, the resists that were typically used for making microlenses do crosslink above a certain temperature [54–56]. Also, resists tend to become brittle and adhere more strongly to the substrate once treated beyond a certain temperature threshold. Typical positive tone resist reflow above 110–130 °C and embrittlement starts to occur

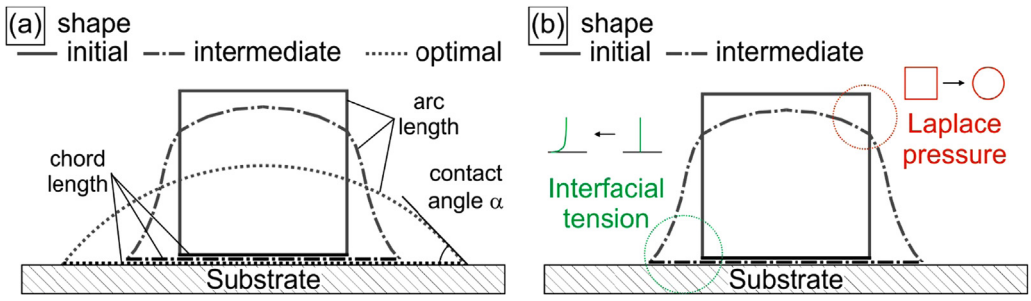

Fig. 3. Schematic of the shape evolution of a box-type line cross-section into: **(a)** an intermediate state and a final optimal lens-like state having the same contact angle α but highly differing from each other in shape and overall systems energy. (reprinted with permission © IOP/JMM) [64] **(b)** an intermediate state as an illustration of the pure Laplace effect on the corners (red) and the combined Laplace / interfacial tension effect (green). (For interpretation of the references to color in this figure legend, the reader is referred to the web version of this article.).

due to reaction with ambient oxygen beyond 130 °C and increased adhesion as well as cross-linking starts above 140 °C [56]. The recommended reflow temperature for these materials is thus in the range of about 110–135 °C [56]. This leads to the fact that the contact point or line between resist and substrate is can remain fixed and does not move, which can be a limitation of the possible lens shapes. Furthermore, the cross-linking counteracts the reflow. Thus, not all initial shapes can be transformed into energy optimal and microlens shapes [55,57]. The reason is that the reflow yielding the ideal continuous curvature lens shape, is slow compared to the crosslinking process [55].

In addition, the non-exposed positive photoresist has still a low M_w, thus there is *no* visco-elastic plateau beyond the softening point at T_g (Fig. 2). This is the so-called molecular-mass independent plateau of the relaxation modulus [93]. Thus, the reflow proceeds rather fast once the softening temperature is exceeded upon heating. By using thermoplastic polymers with a well-controlled molecular weight with a significant visco-elastic plateau, reflow becomes a slow and rather well controllable process. This means a control of viscosity and thus speed of transformation is possible by adjusting the reflow temperature T_{reflow}.

3.2. Advanced reflow process: material contrast

The composition of typical linear thermoplastic materials such as PMMA is rather simple compared to typical photoresists used for reflow. It softens once heated above a specific range of temperature defined by T_g. Significant flow only starts in a regime some 20–60 K above T_g, where viscosities are low enough that deformation can be performed with a nearly viscous behavior. This is due to the amorphous characteristic of PMMA. Crosslinking processes do not exist within the typical temperature regime used for reflow being at and also significantly beyond the glass transition temperature (T_g + 100 K). Thus, the surface tension-driven reshaping acts without significant competition by another process (cf. Section 3.5). Thus, time and temperature can be fully exploited as variable parameters to tune the reflow results. In addition to time and temperature, the initial geometry and the material contrast serves as another variable controlling the reflow shape. The latter one provides different molecular weights and thus viscosities at a given reflow temperature within the same fabricated structure.

3.3. Energy based description of the reflow process

The reflow process follows energy minimization and can be described as surface energy driven flow or in other words creep process. The constant wetting or capillary force acting on the mobile polymer network creates a continuous polymer movement until an energy optimum is reached, i.e., equilibrium at which no further flow occurs and the shape is stable. This is achieved when the lens has a continuous curvature profile and the contact angle at the triple phase line of ambient, polymer and substrate reaches the value defined by the surface free energy of the polymer and the substrate. The system tries to minimize its total energy, which can be analytically described by surface energy terms. This description depends on the material system of interest. It might involve different energy contributions for curvature modeling. Often the temperature can be adjusted high above T_g for fast reflow to a stable terminal shape or to moderate temperature with slower flow where it is possible to achieve intermediate shapes. It has to be noted that the constant curvature and macroscopic contact angle criterion might follow different time scales [64]. The slowest process determines the time to equilibrium. According to Abe et al. [60] and O'Neill et al. [61] in the case of the photoresist reflow, the strong molecular interaction and cross-linking processes during reflow require an additional surface curvature term extending the classical Laplace theory to sufficiently describe the typical final aspheric lens shapes obtained by photoresist reflow. This so-called curvature correction model is a macroscopic, geometric description that can be used to fit experimentally observed lens profiles, extract respective parameters and predict the reflow behavior. Basically, all energy contributions can be ascribed to surface properties and do not required bulk or volume treatment [60] and thus allows for a full analytical treatment.

Fig. 3 depicts the transition between the initial shape and the final shape (cf. Fig. 7) via an intermediate shape. The reflow starts with corner rounding due to the Laplace pressure within the polymer as well as movement of the foot along the substrate due to the interfacial tension and forces between the substrate and the polymer (wetting). The final shape is defined by a constant curvature and the contact angle between polymer and substrate.

The reflow of PMMA as already discussed follows different boundary conditions. Most important, constant curvature shapes are obtained after reflow for the final shapes. In terms of the curvature correction model discussed above, the analytical theory reduces again to the classical Laplace theory. Important to note is that depending on temperature and time, aspherical shapes can be obtained as intermediate shapes. This means the contact angle criterion might be fulfilled while the mean curvature criterion is not. This was expressed by two decay constants for the contact angle and for an arbitrary ratio using the contour length in previous work [64]. A curvature correction approach might be considered for those intermediate states. However, the energy-optimized shape will always be a spherical and constant curvature shape. The surface energy terms in the model involve the lens surface free energy and thus Laplace theory (curvature criterion) as well as interfacial energy (contact angle criterion).

3.4. Simulation of reflow

There are different approaches for simulation of complex flow phenomena like polymer reflow. In all cases, the governing physics being surface energy flow have to be considered. In the following, we show two examples: (i) an analytical solution and (ii) numerical finite element based simulation.

Leveder et al. [62,63] used an analytical, spectral approach to describe the reflow behavior of periodic isodense lines with varying periods (or spatial frequencies). This approach clearly confirmed that high-frequency features such as small period isodense lines reflow faster than larger periods. The same is true for isolated lines. A *rect*-shape (box-type) in the spatial domain with infinite amount of higher order frequencies in the spectral domain will quickly decay towards a *sin*-like

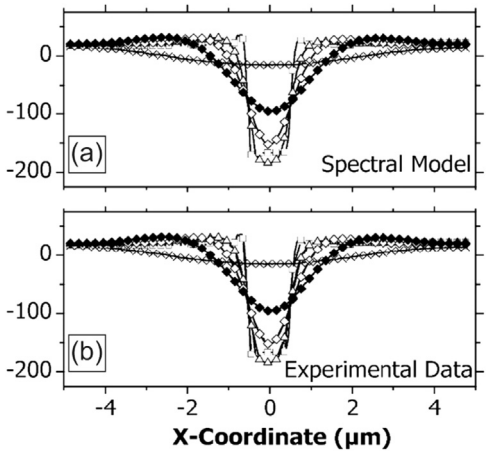

Fig. 4. Reflow simulation obtained with the spectral model of Leveder et al. [62] for a polymer trench capturing very well the early state of reflow as the direct comparison with the experiment shows. (reprinted with permission © AVS/APL).

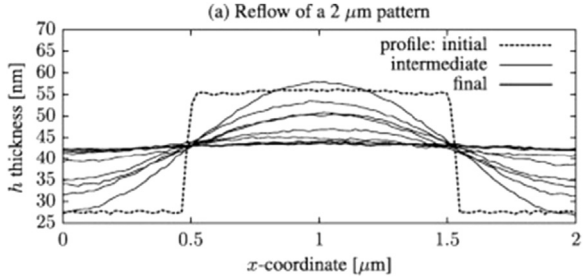

Fig. 5. Reflow simulation obtained with the spectral model of Leveder et al. [63] for a polymer line on a support capturing also very well the early aspherical state of reflow as the direct comparison with the experiment shows. (reprinted with permission. © Elsevier/MEE).

shape (sinusoidal-type) due to vanishing of higher frequencies. Figs. 3, 4 depict the analytical calculation for an isodense polymer trench (Fig. 4) as well as line on a polymer support (Fig. 5) with clear early state, aspherical shapes during reflow. Due to the polymer support, this calculation does not require a contact angle consideration and follows purely the Laplace theory.

In case there is no support, the simulation model changes drastically as the interfacial energies (contact angle) must be considered. We showed [64,65] that isolated lines can be simulated using for example, computational minimum resource methods such as soap-film techniques as for example the Surface Evolver (SE) software [66]. The SE soap-film simulator was already used for simulation of solder reflow [67], droplet microfluidics [68], and self-alignment by wetting [69]. In this case only the initial and the final shape were of interest. However, in the case of the slow polymer reflow, also the intermediate steps can be determined by the soap-film method for complex systems involving multiple viscosities or mobilities (Figs. 7, 8).

The SE concept is special in the sense that is only works with surfaces and ascribes all bulk-properties to these surfaces. This gives some limitations, especially when bulk effects such as elastic behavior are important. Other simulation methods use finite element volume methods [70], which allow for covering the full range of possible bulk effects. The soap-film method purely follows energy optimization criterions that resemble very well the energy optimization steps in a slow reflow process. As explained above, for the PMMA reflow the Laplace theory describes sufficiently well the reflow behavior without the need for curvature correction models for final reflow shapes. Fig. 6 exemplifies the 3D soap-film simulation for an isolated line with a finite element meshing of the contour (polymer surface) and an *empty* interior.

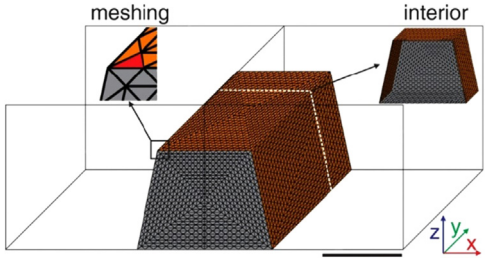

Fig. 6. Mesh for the simulation of an isolated line with the Surface Evolver soap-film methods using only interface and surface properties without simulating the interior volume part. (scale bar 1 µm). (reprinted with permission © IOP/JMM) [64].

As can be seen from Fig. 7, the SE simulation represents very well the constant curvature shape as well as the evolution over time. In this case, the arbitrary r-parameter described the deviation of the curvature from an ideally spherical shape. The linear relation between simulated time and real time allows for a fit of the simulated shapes with the experimental shape. Please note that for this simulation only the contact angle over time was prescribed for the simulation as obtained from experiments to get the correct real-time relation. The final contact angle $\alpha_\infty = 27^\circ$ originates from the unknown and not accessible surface free energies of the system of investigation and thus from experimental observation. The initial angle between sidewall and substrate was $\alpha_\infty + \Delta\alpha = 76^\circ$. The deviation between simulation and experiment for the 480 min reflow stems from the simulated final contact angle in comparison to the experimentally observed value being about 27° in the simulation and 21° in the experiment. For this reason, the final shape is already reached after 240 min with no significant change anymore until 480 min. Due to the high reflow temperature of 120 °C, being well beyond the glass transition temperature of the exposed region (estimated T_g 94–100 °C), the lens quickly assumed the constant curvature shape. For single lines, limitations of this method are still early phase states during reflow. To cover these early states, additional model improvements are required.

The use of different methods with surface energy consideration discussed above showed already resource efficient and still quite correct simulation. However, so far only a homogeneous and constant material behavior of reflow regions was considered. As discussed in the following, this is necessarily not always the case. From a practical point of view, structures with material contrast are of much larger interest and are seldom covered by other simulation methods so far.

So far, we only considered isolated and thus independent structures. In practical situations, most of the structures will be placed in periodic arrays. The reflowing structures remain only independent as long as they are separated by a free space on the substrate. As soon as different structures contact each other and merge during reflow, there is a complete change in the reflow regime. The substrate itself has then no influence – as long as the polymer films remain thick enough and for example dewetting effects are not of relevance. Once the substrate surface is covered by the reflowing polymer, only the mentioned Laplace effects have to be considered. In principal, the model simplifies to the also above-mentioned spectral considerations for reflow on supported films. Actually, the polymer film acts as a wetting enhancement layer because the polymer-polymer contact angle is lower than the polymer-substrate contact angle. In conclusion, this means that for a reliable fabrication of blazed gratings for example, a minimal gap between the prisms has to be maintained to ensure optimal optical functionality. This can, e.g., be done by mechanical or chemical means [71].

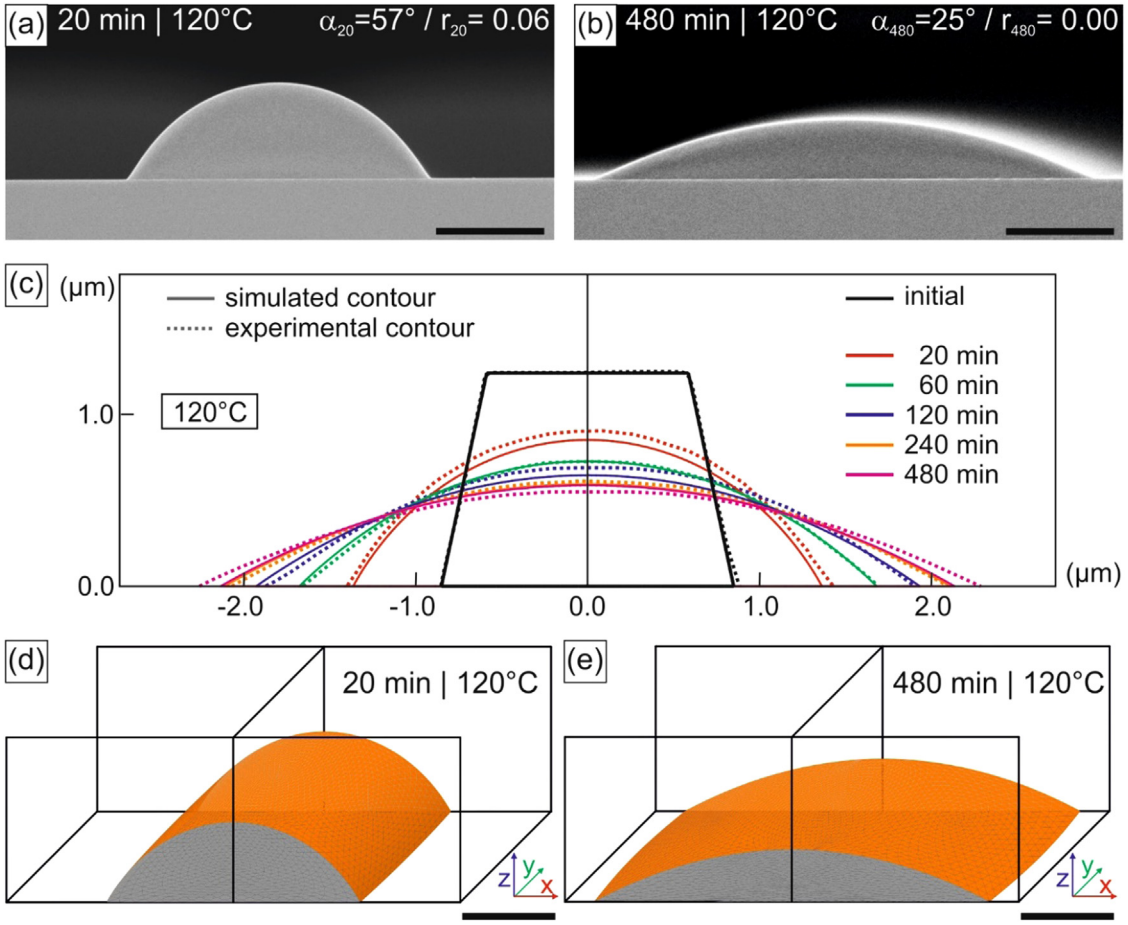

Fig. 7. Comparison of **(a)** and **(b)** experimentally obtained scanning electron microscopy (SEM) cross sections and **(c)–(e)** simulation of single (isolated) 100 µm long and 1700 nm wide lines reflowed for different times at a constant temperature (scale bar: 1 µm) (simulation parameters: $\alpha_\infty = 27°$, $\Delta\alpha = 49°$, $\tau_\alpha = 3108\,s^{-1}$, exponential contact angle decay assumed). (reprinted with permission © IOP/JMM) [64].

3.5. Dynamic material composition reorganization during reflow

The above-simulated reflow is based on the generation of low M_w polymer chains in the entire volume of exposed resist down to the substrate for high- energy probes. For vacuum UV (VUV) exposure for example, a strong gradient of material properties from the surface to the bulk is generated. For very efficient probes such as photons, the M_w is strongly reduced, even below the limit of volatile fragments. This is for example used in characterization of laser pulse shapes [72–75]. Only fragments that are too large to vaporize are remaining in the bulk or on the surface. During exposure, the volatile fragments directly evaporate into the ambient, in particular when they are near the surface. Other low M_w fragments stay in the bulk of the resist, are concentrated near the surface and will only slowly diffuse. This diffusion will typically occurs after the exposure depending on the ambient conditions. Such fragments just behave like very good solvents due to their structural compatibility and diffuse into the high M_w regions. The diffusion depends on the properties of the linear polymer network and there is a significant mobility even in solid-state linear polymer networks [76]. The low M_w fragments move into between the polymer chains (homopolymer diffusion) especially at increased temperatures. Thus, during the reflow there can be a competing process to the material displacement. The low M_w fragments mix with the polymer network and effectively change the M_w of the interface region first and later of the full polymer region depending on the diffusion conditions (e.g., temperature and time).

Fig. 9 emphasizes the effect of homopolymer diffusion for vertical contrast generated with VUV exposure. Fig. 8a,b show the unexposed situation for a thin PMMA film where a rough to medium-smooth cross section was obtained upon manual, crystal oriented cleaving of the silicon substrates. There is a certain surface layer of about 150–350 nm of unknown origin so far. The layer thickness depends on the annealing and time between stabilization and measurement. However, the important point is that the total film is more or less homogenous despite this very different top layer. After VUV treatment, about 110–120 nm film thickness is lost directly due to vaporization of low M_w fragments and the unclear top layer also vanished (Fig. 9). The essential part is that without any additional heat treatment a clear modified surface is visible with increasing M_w towards the substrate. Indicative for this is the increasing granularity in Fig. 9c from top to bottom with a clear difference in the superficial region of 300–500 nm [77]. This is the visualization of the vertical material contrast. With heat treatment, the complete film changes its M_w and becomes completely homogeneous in its M_w distribution from top to bottom again (Fig. 9d). When comparing Fig. 8c and d, there is a clear loss of about 400 nm PMMA due to the stabilization (hardbake) of the film at 165 °C. During exposure, the surface temperature did not exceed 50 °C. In addition to the diffusion, we assume that even more and larger fragments left the surface due to vaporization. Alternatively, there might be a compaction of the film.

In context of polymer reflow, the consequence of this behavior is a dynamic change of the reflow behavior during reflow. For certain situations, the reflow might even come to stop as the average M_w and thus the T_g increases above a certain threshold T_{th} and thus the used reflow temperature. As a consequence, not only the top surface or a certain region has a lowered T_g. The complete structure might be different in its mechanical properties before and after reflow. In general,

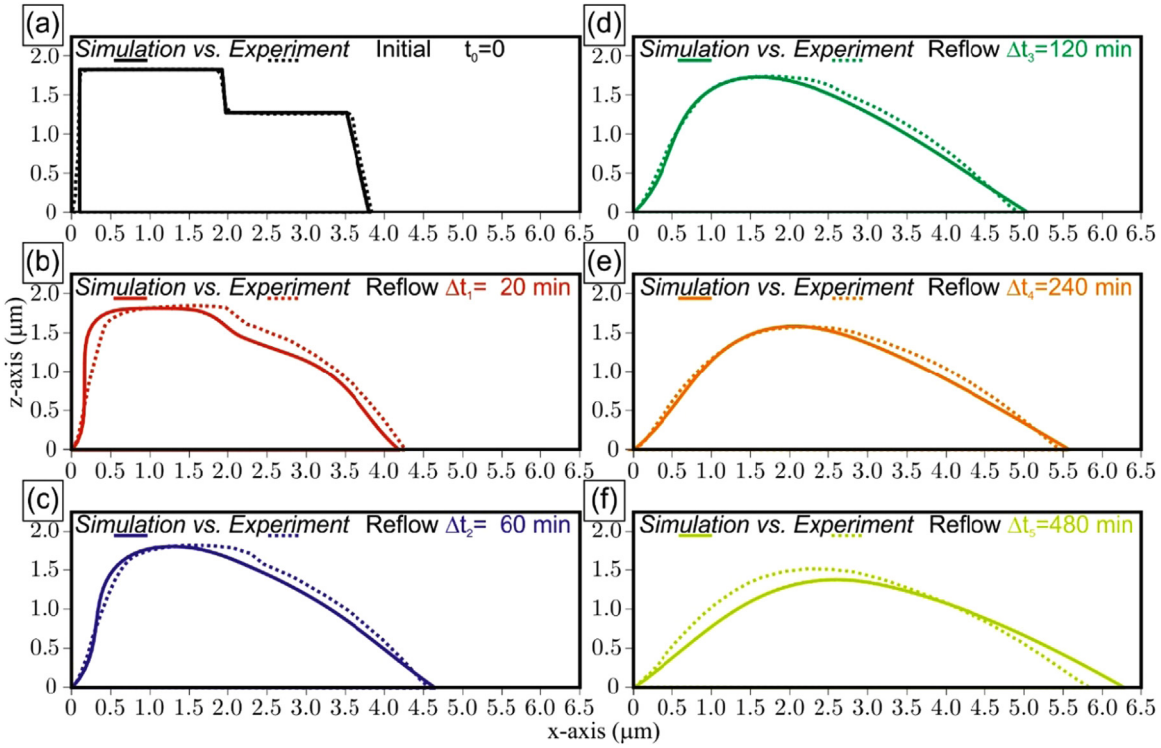

Fig. 8. Simulation and experimental verification of a double step structure reflowed at 120 °C where the left-step has a 5-times lower mobility than the right step. (reprinted with permission.visco © AVS/JVST).

the material contrast has been reduced due to diffusion effects of the low M_w fragments. Depending on the used processes (initial contrast, temperature of reflow, size of features), the material contrast might have been almost vanished as depicted in Fig. 9d.

In the before discussed examples, one has to note that this effect is much stronger in VUV exposure than in the EBL exposure because of the much smaller M_w fragments for the VUV exposure. Also in the EBL, this interface broadening and mixing affects the final reflow shape and can be considered as a kind of uncertainty and thus deviation from the ideal reflow assuming non-intermixing interfaces. However, the differently exposed regions remain clearly separated (cf. Fig. 10). The reflow times were relatively long. So, the contrast between the different M_w regions was not sufficient to enable significant diffusion. For this situation, the reflow simulation without mixing, as shown in Section 3.4, deviates only minimal from the real experimental situation.

4. Applications of selective reflow

4.1. Overview on 3D surface topographies

Typical 3D applications with special attention to selective reflow can be broadly divided in three categories: (A) structures where stepped features and surface features are smoothened out to continuous profiles while the overall shape, or the “geometric envelope”, is preserved, (B) hybrid structures in which smoothening is locally restricted and other micro- and nanostructures can be preserved, and (C) structures in which dislocation of entire elements can be initiated. The first case (A) is nearest to the classical lens reflow. However, here we focus on applications where *asymmetric* structures with different slopes and resolutions are needed. Case (B) requires a selectivity not only on the localized reflow, but also involves additional structures which are excluded from reflow because their structuring does not involve a reduction in M_w. Case (C) presents cases where capillary flow and collapse of entire structures leads to possibilities to modify entire shapes. This is nearer to evolving origami methods of self-assembly than to rearrangement of structures, where the “geometric envelope” remains similar during the entire process.

4.2. Continuous profile surfaces: from surface approximation toward ideal representation

In contrast to discrete profiles being ideal for a fabrication with grayscale lithography methods, analog or continuous grayscale profiles are a particular challenge for such grayscale methods. Directly printing them would require either a continuous dose distribution or a highly resolved discrete dose distribution that becomes quasi-continuous throughout the process. Reflow is able to easily transform fabricated discrete profiles into ultra-smooth and fully continuous profiles. Fig. 11a-c show exemplary discrete step profiles realized by GEBL in PMMA in a one-step lithography approach (single exposure and single development). Fig. 11d-l show the transformation of those profiles into increasingly continuous profiles by heating the structures at 120 °C for different times. Because the process is slow, all intermediate steps can be accessed just by cooling the structure back to room temperature after a given time. In all cases the left most pillar is not exposed at all (initial M_w, visible by the strong granularity of the cleaved facets). In the multistep patterns in Fig. 11c,f,i,l, a discrete reduction of M_w can be seen for increasingly lower resist levels due to the higher dose used to make these levels via GEBL. In consequence, the lowest level hast the lowest T_g and thus reflows at the lowest temperature and fastest at a given temperature. In any case, the unexposed pillar either does not move at all or is only deformed (“pulled over”) by capillary forces of the flowing section of the structure. All subset pictures in Fig. 11 show how an asymmetric initial structure (in geometry and T_g) can be used to generate asymmetric structures such as asymmetric optical prisms and micro-lenses. The shown structure would require diffractive optical designs or very small wavelengths (kinoform x-ray lenses) but similar things can be done using larger resist films and bigger structures. In this case, also grayscale photolithography instead of GEBL can be used.

The optical efficiency of continuous profiles is higher than the one

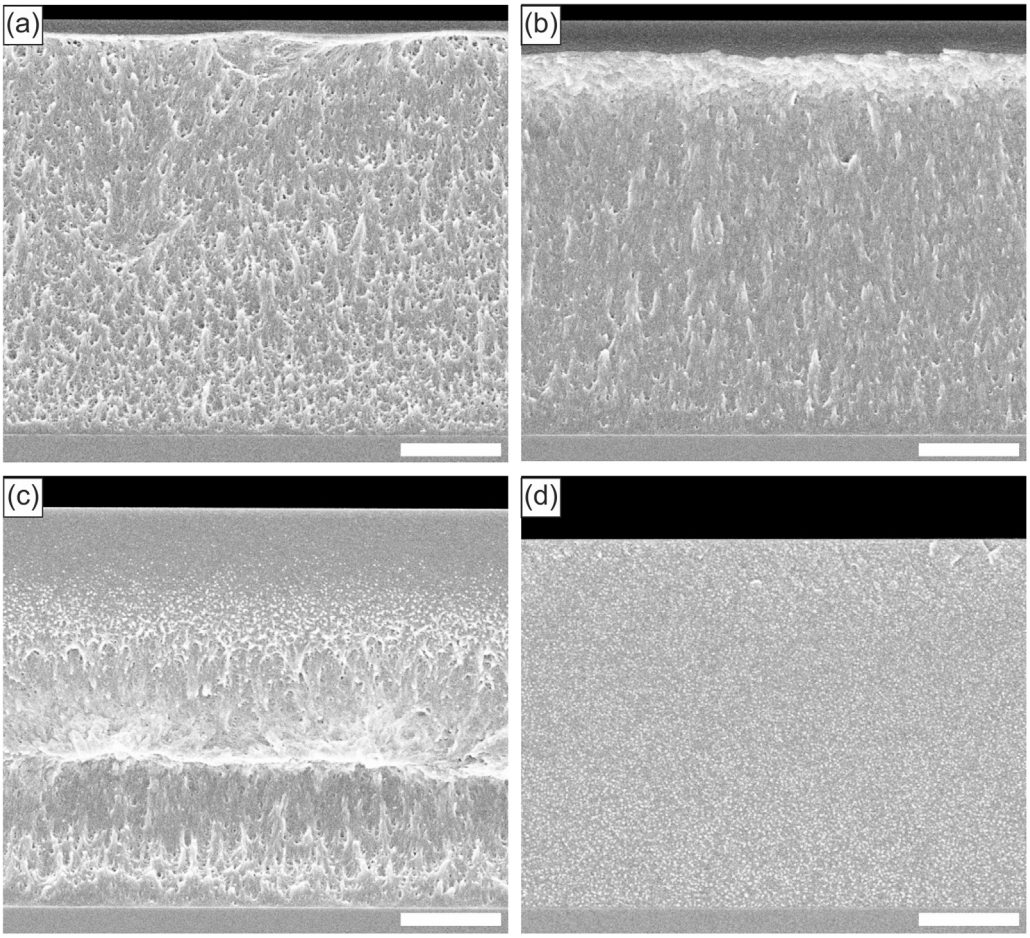

Fig. 9. SEM micrographs of PMMA cross-sections **(a)** annealed after spin-coat for 2 min at 140 °C (M_w ~ 100 kg/mol, T_g ~ 122 °C), **(b)** annealed after spin-coat and stabilized before measurement for 70 min at 200 °C (M_w ~ 100 kg/mol, T_g ~ 122 °C), **(c)** annealed after spin-coating and VUV exposed without further treatment (average T_g ~ 50 °C), **(d)** stabilized after spin coating, VUV exposed without further treatment and stabilized for 70 min at 165 °C before measurement (average T_g ~ 50 °C) (scale bar 1 μm).

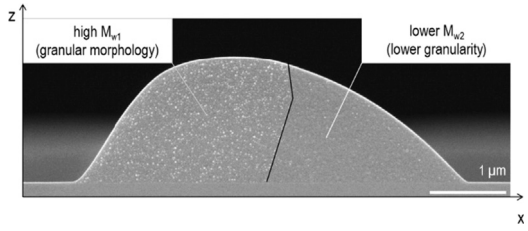

Fig. 10. SEM micrographs of PMMA structure written by GEBL and reflowed at 120 °C for 120 min with clear pull-over towards the low M_w section along the x-axis but without significant change of the M_w distribution along the interface (solid black line) between the high and the low M_w regions. The kink in the solid black line clearly indicates the initial step position between both regions (cf. Fig. 11b).

for multilevel diffractive elements [78,79]. However, the fabrication of continuous profiles by methods such as laser direct writing or polymer reflow is also more challenging than for multilevel designs. In continuous profile fabrication, the loss in efficiency due to improper process control can easily cancel out the efficiency improvement of continuous designs. For example, the deformation of the highest step in Fig. 11 reduces the optical efficiency due to so-called dead blaze regions [new21]. Reasons for the deformation are (i) the high reflow temperature required for the second highest step being close to the T_g of the unexposed step and (ii) the capillary force created by the reflowing section (cf. Section 4.4). While the first effect can be minimized, the second one offers little room for improvement. In the demonstrated examples, the achieved T_g range is directly linked to the GEBL to have a simplified process. There is some room for improvement within a single-step process by using higher exposure doses that will in general lead to faster resist dissolution of the exposed sections. This usually reduces the process accuracy for simple practical reasons: handling times become more process dominant. Slower development processes (developer concentration and temperature) can counter balance this. A further detailed discussion of EBL process control is outside the scope of this review. Further process insights especially on process and material optimization for high-resolution EBL as well as chain fragmentation can be obtained for example from references [80–88]. By using an aligned second EBL exposure on the developed discrete profile one can further reduce the T_g in the already exposed region enhancing the T_g contrast compared to the unexposed stable region (cf. Fig. 17c and text). This will minimize the deformation of the highest step even though the process becomes more complex. Important to note is that reducing the width of the largest step will reduce the non-active optical region but will also increase the deformation of the largest step by capillary forces and thus the dead blaze again. In conclusion, a certain dead blaze cannot be totally avoided with the combination reflow and GEBL. The final application defines the used technique and it might be well a non-optical one.

For the reflow outcome, the initial geometry is most important. The relation of width and height define whether the Laplace effects (corner rounding) or the interfacial effects (wetting) dominates the overall shape transformation. For comparable width and height as in Fig. 11

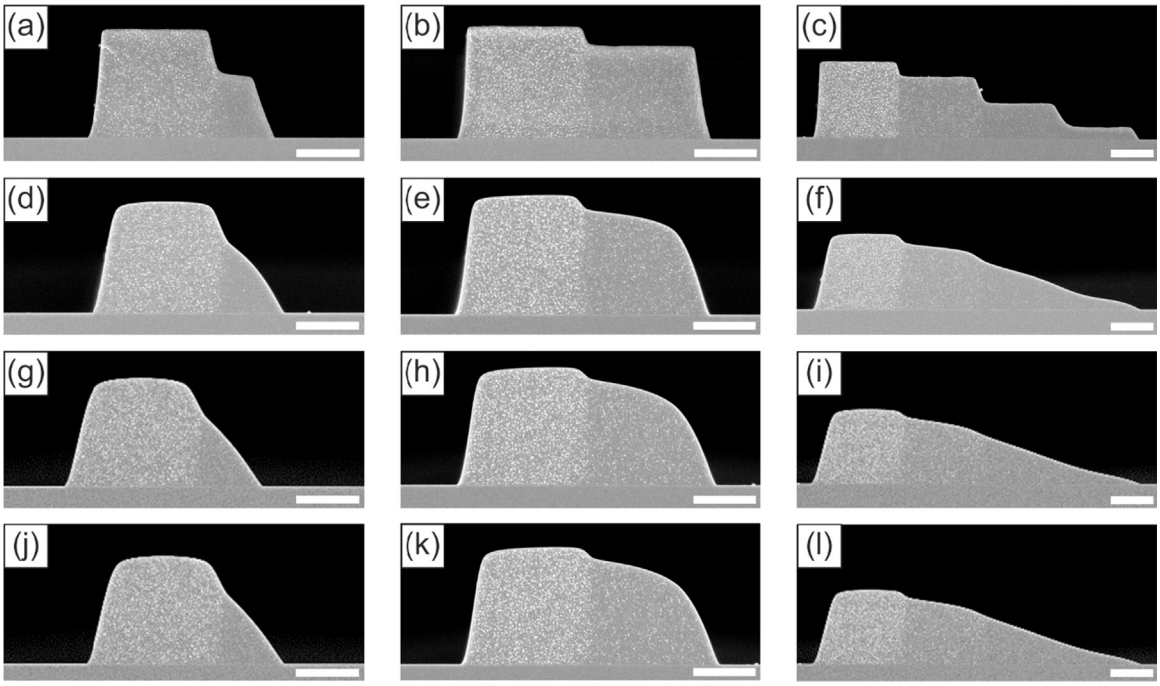

Fig. 11. SEM micrographs of asymmetric PMMA patterns using GEBL and reflow: (a-c) initial, (d-f) 20 min reflow at 120 °C, (g-i) 60 min reflow at 120 °C, (j-l) 120 min reflow at 120 °C. (scale bar 1 μm).

both effects are similar in contribution.

The described reflow process is rather generic and can be used for all thermoplastic materials that allow a modification of its T_g. Fig. 11 gives three examples of patterns realized in PMMA (Fig. 12a,b), a positive tone and typical electron beam resist in research, mrPosEBR (Fig. 12c,d) [89,90] as alternative resist with good etch selectivity, and ZEP520A (Fig. 12e,f) [15], an example for a highly sensitive and high-resolution resist interesting for fast production and industrial use. Fig. 11 also shows the reflow behavior for different reflow temperatures in relation to the unmodified resist T_g. PMMA has a T_g of about 122 °C [36] and the reflow took place at 120 °C – just below T_g – for 120 min. Mostly the exposed steps are reflowed without significant movement of the left most step. The mrPosEBR hast a T_g of about 125 °C and a reflow for 20 min at 125 °C – just at T_g – for 20 min only was already sufficient to completely remove the steps and also effect the left most step. ZEP520A has a T_g of about 120 °C but the reflow proceeded at 150° – well above T_g – for 20 min only. Due to the high temperature the structure was strongly deformed including the left most step.

As mentioned before, the reflow depends on the dimensional relations: Reflow can, thus, also be used to smoothen surfaces without deformation of the overall shape, i.e., to remove surface roughness while preserving the steps defined by GEBL. While in the figures above the step widths were in comparable size to the step heights, in Fig. 13 a much thinner resist film is shown. First, it becomes clear that well controlled step patterns with sub-6 nm steps can be realized in 30 nm thin PMMA by GEBL. The AFM shows a significant roughness that is believed to originate from the relative large initial M_w (100 kg/mol) with a wide M_w dispersion [36]. Especially lower levels have an increased roughness. This is also a known effect for GEBL. Small deviations in dose and material composition become more visible for long development times and for smaller total M_w. By heating the structures for about 20 min at 110 °C and 120 °C, and thus above the T_g of the steps, this roughness vanishes without effecting the step-structure significantly. Only for longer reflow times the step-patterns would be transformed in continuous profiles just as in Fig. 12. To understand this, one hast to see the much larger step-width compared with the step-height that requires a relative long material displacement before structural deformations towards a continuous profile can be seen. Basically, the PMMA hast flow for a much longer distance before "stretches" the steps between the largest step and the flowing material front. In addition, there are reports on the thin-film effect on the PMMA T_g depending on the substrate interaction [91]. This makes it difficult to relate the results in Fig. 13 exactly to the observations in Fig. 12.

4.2.1. *Surface-selective reflow – photon based polishing process*

The smoothening observed for the nano-steps before (cf. Fig. 13) can be also used at the micro-scale. In this case it was supported by the additional creation of a low T_g "skin" region (Fig. 14a) on top of the

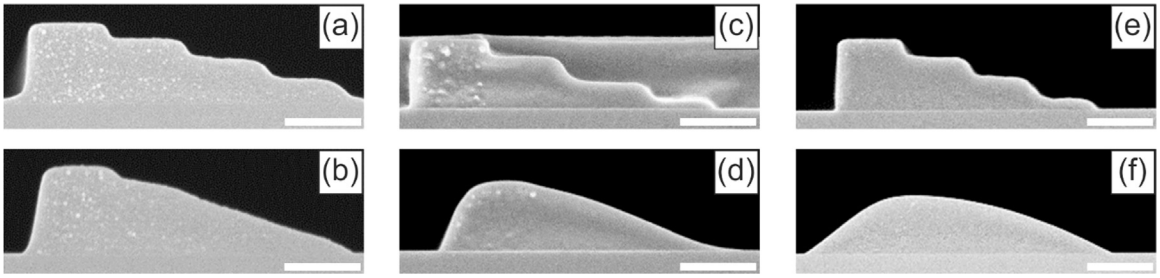

Fig. 12. SEM micrograph of PMMA multistep profile with about 500 nm wide steps in 450–500 nm thick polymer films realized by GEBL: **(a-b)** PMMA initial and after reflow for 120 min at 120 °C, **(c-d)** mrPosEBR initial and after reflow for 20 min at 125 °C, **(e-f)** ZEP520A initial and after reflow for 20 min at 150 °C.

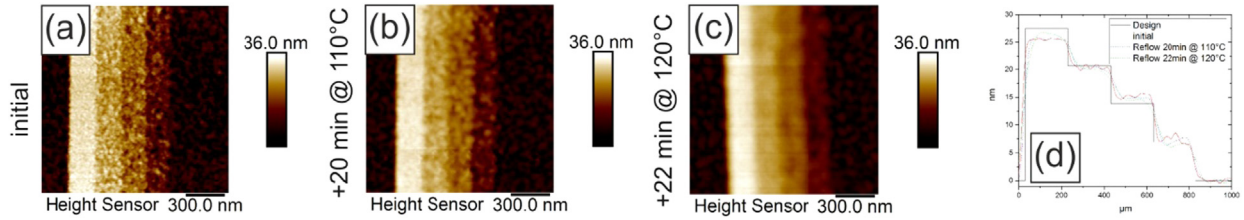

Fig. 13. Atomic force microscopy (AFM) images for the surface smoothening without step relocation: **(a)** initial pattern in about 30 nm PMMA film, **(b)** same pattern after 20 min reflow at 110 °C with smoothening already of the lowest steps due to reduced T_g of those steps, **(c)** similar smoothening after additional 22 min reflow at 120° and in addition first displacement of the largest step along the x-axis due to onset of capillary force based reshaping, **(d)** cross sections for multiple-line averages of the micrographs (a)-(c).

50 µm tall micro-lens. For this, the initial lens printed by multi-photon-lithography was replicated with a soft mold into PMMA [92]. This allowed for the VUV exposure of the PMMA and a subsequent selective reflow of the top region only *and* without any effect on the bulk [8]. This means that surface undulations in the size range of the modified depth (300–500 nm) were smoothened out while the total geometry (a concave microlens with 40 µm sag with sharp tips between adjacent lenses) was not affected.

4.2.2. *Surface mechanics – making use of continuous profiles*

Another continuous surface profile application is bioinspired surfaces of animals that move through granular media such as sand with reduced solid-state friction in one preferred direction. To fabricate similar engineered, bioinspired surfaces we combined GEBL, thermal reflow, polymer replication techniques and ceramic replication [94,95]. Fig. 15a shows the initial patterns after GEBL in different views. For typical applications, large areas are important and the GEBL process was optimized for fast writing, involving only few grayscale levels with relatively coarse resolution. Fig. 15b shows the same surface after reflow for 5 min at 130 °C – well above the T_g of the used PMMA. The quick post-processing was able to completely reduce the discrete character and the writing induced roughness. Thereby, an effective

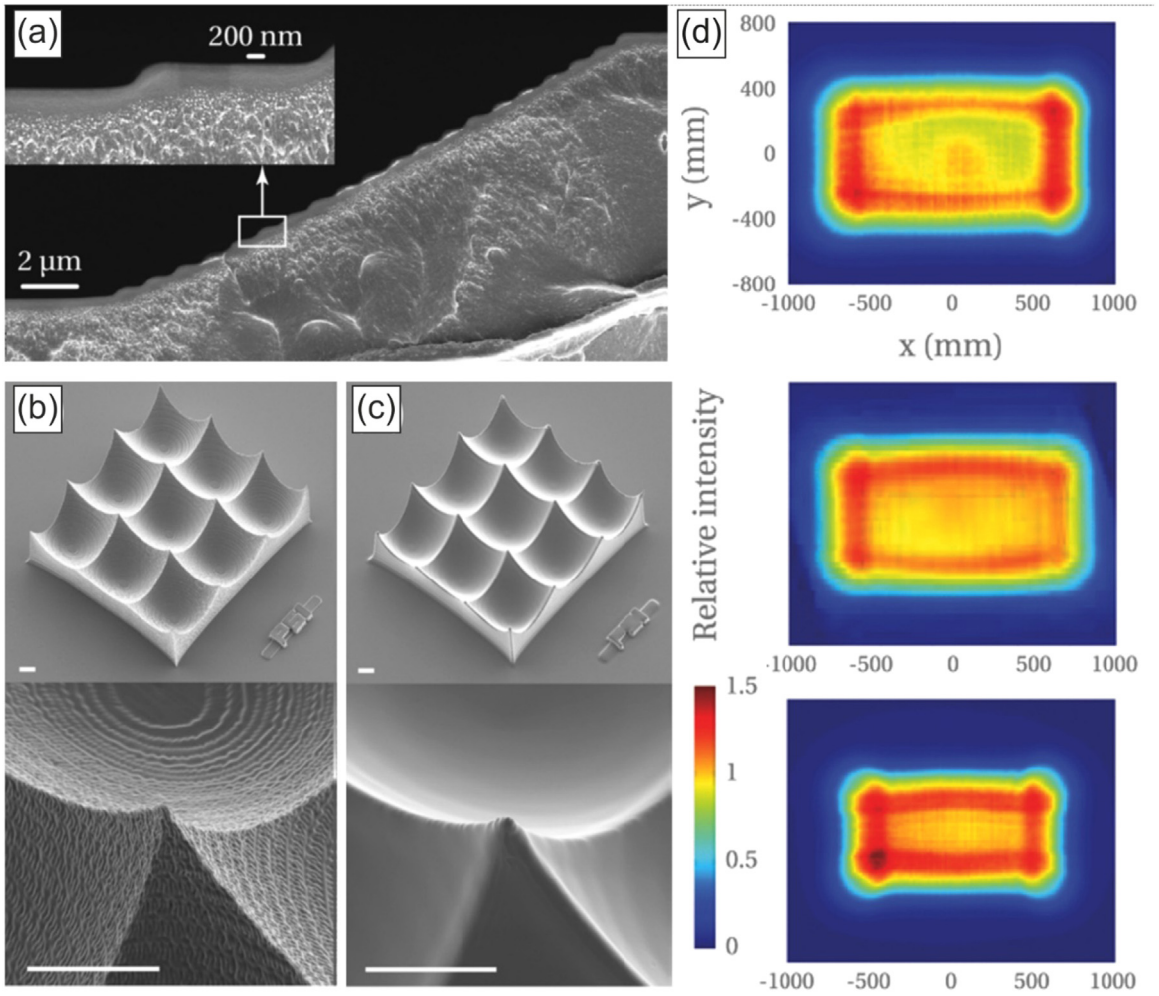

Fig. 14. SEM micrographs for PMMA microscopic structures **(a-b)** before and **(c)** after reflow: **(a)** cross-section of VUV created low M_w and low T_g section on top of unmodified bulk section for a microscopic step profile, **(b)** 3 × 3 lenslets after replication in PMMA, **(c)** VUV exposed and reflowed surface with ultra-smooth surface finish and minimal effects on the total (bulk) geometry and **(d)** optical measurements for different lens arrays: (1) before smoothening as in (b), (2) after VUV exposure and selective smoothening as in (c), (3) only reflow without selective exposure. (scale bar 10 µm) (reprinted with permission © Wiley/AVMT) [8].

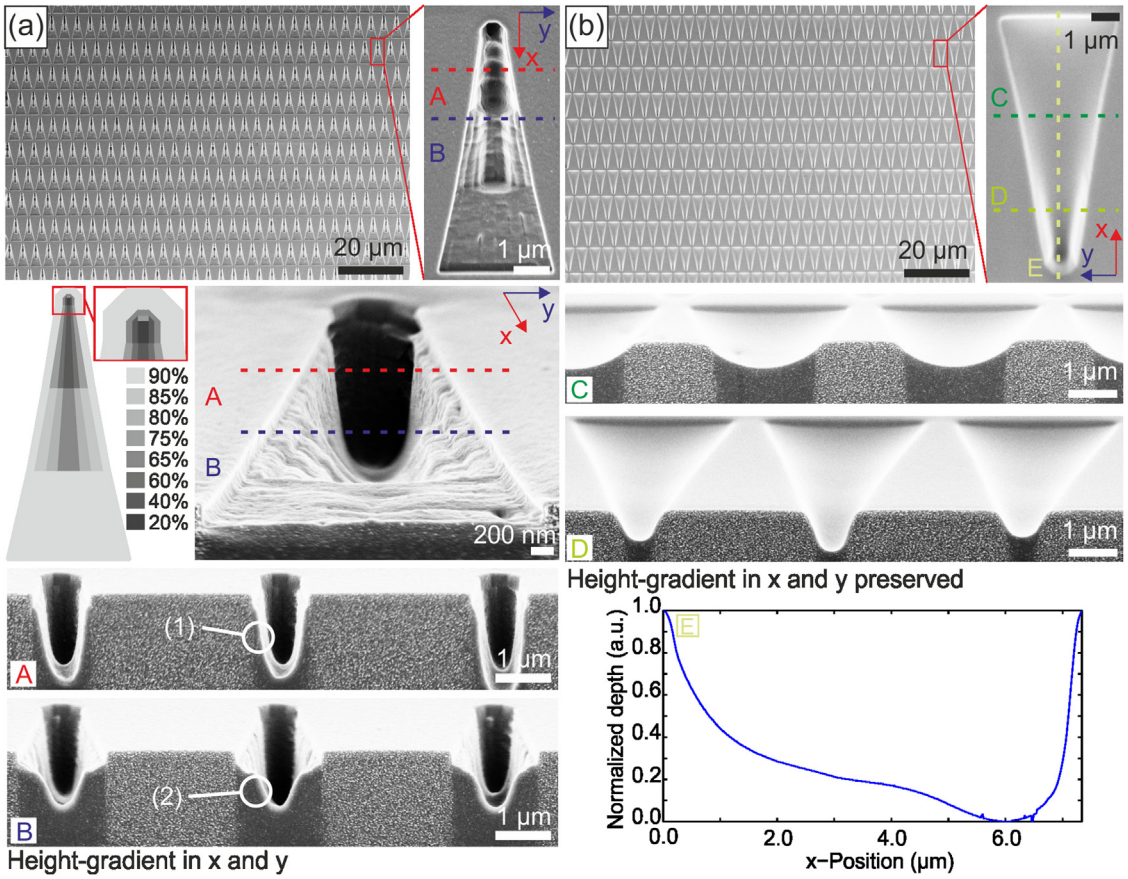

Fig. 15. SEM micrographs of PMMA surfaces **(a)** directly after GEBL and development (large area, zoo-in, relative height pattern, tilted view and cross-section), **(b)** after additional 5 min at 130 °C for reflow (large area, zoom-in, cross-sections and AFM scan along long-axis of the funnel) [94]. (reprinted with permission. © Elsevier/MEE).

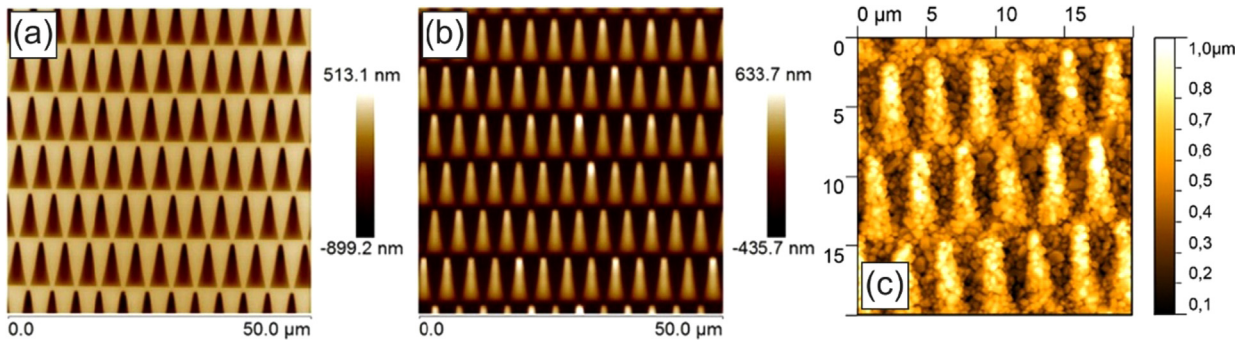

Fig. 16. Atomic force micrographs of **(a)** the reflowed PMMA used as master for further replication steps, **(b)** intermediate mold during replication cycle and **(c)** final patterns transferred into ceramic material after additional intermediate replication steps [95]. (reprinted with permission. © Elsevier/MEE).

fabrication of very smooth surfaces with different geometrical slopes as being required for solid-state friction reduction was realized in a ceramic material. Even with the large granularity of the ceramic, the solid state friction could be reduced by about 16% [95]. Fig. 16a shows the PMMA original used as initial pattern in the complete replication process. This replication cycle used intermediate molds (e.g. Fig. 16b) to finally transfer the pattern into ceramic material by molding a thermoplastic ceramic precursor and sintering (Fig. 16c).

4.3. Hybrid continuous 3D surface: site selective reflow defined by programmed T_g

The selective modification of the T_g enables hybrid patterns consisting of sharp discrete sections *and* completely smooth continuous sections [36] (Fig. 17). Here the key point is the fabrication of the discrete steps for example by NIL [38,93] or by GEBL [36] first. A second patterning step follows, to create additional initial steps for guiding reflow or just to flood expose some sections desired for localized reflow. In any case, it must be ensured that the discrete patterns of the first step are not affected by reflow. This can be achieved by initial exposure dose and thus specific T_g control. It has to be pointed out once more that exactly the same discrete step-profile can be obtained with different doses and different GEBL processes (developer, time, temperature). In consequence, the same profile can have a different T_g distribution.

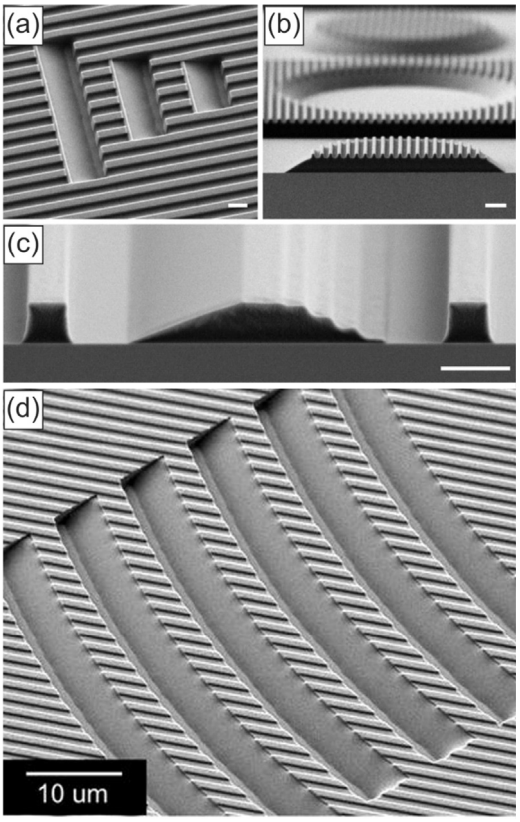

Fig. 17. SEM micrograph of PMMA hybrid patterns realized by a combination of patterning and thermal reflow: **(a-b)** first nanoimprint lithography (binary lines) and then GEBL and reflow (sloped sections), **(c)** GEBL (stepped and cleared regions) and then selective flood electron beam exposure without development and a final thermal reflow (sloped sections), **(d)** example for a pattern used for backlighting (reprinted with permission. © Springer/NanoConv [36] and Springer/APA [93]).

4.4. MEMS actuation: creating forces to move objects

Melting materials to make use of capillary forces to actuate MEMS structures is for example based on melting of metals or alloys [76] having the advantage of high surface tension as well as using polymers [96–102] having the advantage of well controllable properties and modification of polymers as discussed in this review. Capillary forces can be strong enough to align microchips laterally on a substrate [69,103] and to move and place solid plates with respect to each other. The latter one can be done via controlled melting of materials between two solid plates. Fig. 18 depicts an exemplary use of the capillary forces and the softening of polymers at and above their glass transition temperature. Fig. 18a shows the GEBL written pattern with a stable pillar plus a stepped and tapered structure attached to it. This configuration will generate an asymmetric force to the pillar. Fig. 18b gives the situation after reflow. In comparison to Fig. 18a, there is a clearly visible bending of the pillar visible out of its vertical. Fig. 18b gives further details for different temperatures showing an increasing degree of bending for increased reflow times at 120 °C for 5, 10 and 20 min. Longer reflow times translate into more pronounced bending. This is just an outlook into the possibilities that open up using polymer reflow as actuation principle for MEMS structures.

5. Conclusion and outlook

We have shown the underlying principles that control polymer reflow on its molecular level. Mainly, the mobility of polymer chains and the surface forces acting on the polymer chains are responsible for the reflow. A local modification of these properties allows controlling the reflow, either in lateral direction, by use of grayscale lithography, or in vertical direction, by use of surface sensitive exposure. In classical reflow of photoresist, the cross linking limits the freedom of reflow due to a loss of chain mobility and is difficult to control with such materials. In contrast to this, changing the glass transition temperature and thus the mobility of the chains in a linear thermoplastic material at a given temperature allows for a selective reflow. This allows either for novel fabrication methods and post-processing methods of structures or the generation for completely new structures that a not or only very difficult to make in another approach. For example, the shown vertical contrast can be exploited for contactless, radiation-based polishing. In addition, the surface forces and the material relocation associated with polymer reflow can be exploited to actuate microscopic and nanoscopic structures. The most promising aspect here is that the actuation temperature can be modified within one structure using the same actuation material but apply selective modification of this material by different means as shown in this work.

The demonstrated post-processing methods are attractive in multi-material and multi-functional 3D micro- and nanofabrication. This will allows for fabricating reconfigurable and dynamic systems with nanometer precision. Even in the light of multi-material direct printing, the described methods demonstrate a way to directly program certain trigger thresholds by material property control. This is an important aspect of 4D materials, which do exploit time as an additional degree of freedom. All these methods can be used in polymers that allow for a radiation-based modification.

Acknowledgements

Such a review is not possible without the multiple initial contributions that enabled the broad spectrum of applications and simulative investigations of reflow based on T_g gradients – also known as TASTE (temperature activated selective thermal topography equilibration) process – that was summarized in this review. The authors express their

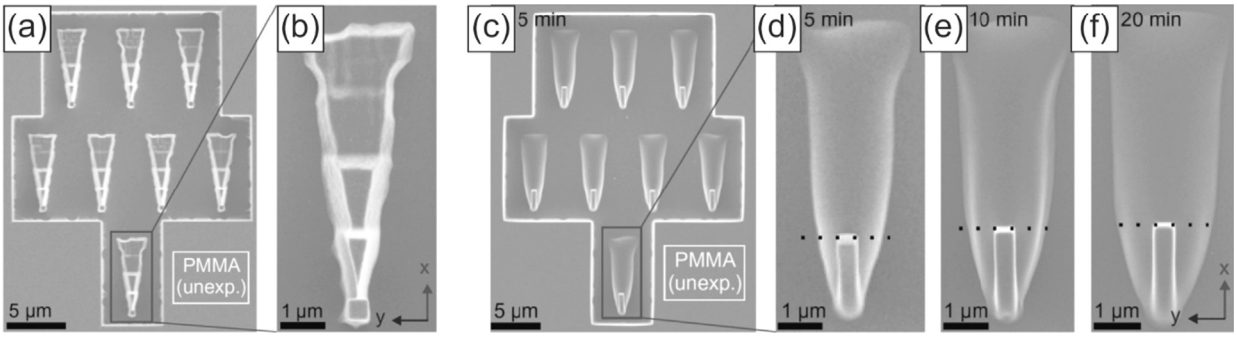

Fig. 18. Bending of pillars due to the capillary forces of the wetting polymer and softening polymer pillar: **(a-b)** initial pattern with zoom in, **(c-f)** after reflow at 120 °C for different times. (reprinted with permission. © Elsevier/MEE).

special thanks to Arne Schleunitz, Christian Spreu, Nachiappan Chidambaram, Mirco Altana, Konrad Vogelsang as well as Remco Smits and Roel Hoekstra for their invaluable contributions over many years. Special thanks are expressed to Vitaliy A. Guzenko for the continuous support of this research over such a long time.

References

[1] Z.D. Popovic, R.A. Sprague, G.A.N. Connell, Technique for monolithic fabrication of microlens arrays, Appl. Opt. 27 (1988) 1281–1284.
[2] F.T. O`Neill, J.T. Sheridan, Photoresist reflow method of microlens production, Part I: background and experiments, Optik 113 (2002) 391–404.
[3] F.T. O'Neill, J.T. Sheridan, Photoresist reflow method of microlenses production: Part II. Analytic models, Optik 113 (2002) 405–419.
[4] K.-N. Chiang, C.-A. Yuan, An overview of solder bump shape prediction algorithms with validations, IEEE Trans. Adv. Pack. 24 (2001) 158–162.
[5] J.O. Choi, J.A. Moore, Degradation of poly(methylmethacrylate) by deep ultraviolet, x-ray, electron beam, and proton beam irradiations, J. Vac. Sci. Technol. B 6 (1988) 2286–2289.
[6] J.A. Moore, J.O. Choi, Degradation of Poly(methyl methacrylate): Deep UV, X-ray, Electron-Beam, and Proton-Beam Irradiation, in: ACS Symposium Series 475, 20XX, Ch. 11, pp. 156–192.
[7] S. Eve, J. Mohr, Study of the surface modification of the PMMA by UV-radiation, Proc. Eng. 1 (2009) 237–240.
[8] N. Chidambaram, R. Kirchner, R. Fallica, L. Yu, M. Altana, H. Schift, Selective surface smoothening of polymer microlenses by depth confined softening, Adv. Mater. Technol. 2 (2017) 1700018.
[9] V.V. Aristov, S.V. Dubonos, R.Y. Dyachenko, B.N. Gaifullin, V.N. Matveev, H. Raith, A.A. Svintsov, S.I. Zaitsev, Three-dimensional design in electron-beam lithography, J. Vac. Sci. Technol. B 13 (1995) 2526–2528 (1995).
[10] D.R.S. Cumming, I.I. Khandaker, S. Thoms, B.G. Casey, Efficient diffractive optics made by single-step electron beam lithography in solid PMMA, J. Vac. Sci. Technol. B 15 (1997) 2859–2863.
[11] Y. Hirai, S. Harada, H. Kikuta, Y. Tanaka, M. Okano, S. Isaka, M. Kobayasi, Imprint lithography for curved cross-sectional structure using replicated Ni mold, J. Vac. Sci. Technol. B 20 (2002) 2867–2871.
[12] N. Unno, S. Yoshida, H. Akamatsu, M. Yamamoto, S. Satake, J. Taniguchi, Three-dimensional hologram-read-only memory duplication by nanoimprint lithography, J. Vac. Sci. Technol. B 31 (2013) 06FB01.
[13] Y. Shinonaga, K. Ogino, N. Unno, S. Yoshida, M. Yamamoto, J. Taniguchi, Fabrication of eight-step diffractive optical element for hologram-ROM, Microelectron. Eng. 141 (2015) 102–106.
[14] S. Zhang, J. Shao, J. Liu, C. Xu, Y. Ma, Y. Chen, N. Taksatorn, Y. Sun, Multistep Aztec profiles by grayscale electron beam lithography for angle-resolved microspectrometer applications, J. Vac. Sci. Technol. B 32 (2014) 06F504.
[15] R. Kirchner, V.A. Guzenko, I. Vartiainen, N. Chidambaram, H. Schift, ZEP520A - A resist for electron-beam grayscale lithography and thermal reflow, Microelectron. Eng. 153 (2016) 71–77.
[16] F. Hu, S.-Y. Lee, Dose control for fabrication of grayscale structures using a single step electron-beam lithographic process, J. Vac. Sci. Technol. B 21 (2003) 2672.
[17] R. Murali, D.K. Brown, K.P. Martin, J.D. Meindl, Process optimization and proximity effect correction for gray scale e-beam lithography, J. Vac. Sci. Technol. B 24 (2006) 2936–2939.
[18] S.-Y. Lee, K. Anbumony, Accurate control of remaining resist depth for nanoscale three-dimensional structures in electron-beam grayscale lithography, J. Vac. Sci. Technol. B 25 (2007) 2008–2012.
[19] C. Guo, S.-Y. Lee, S.H. Lee, B.-G. Kim, H.-K. Cho, Application of neural network to controlling three-dimensional electron-beam exposure distribution in resist, J. Vac. Sci. Technol. B 27 (2009) 2572–2579.
[20] W. Mi, P. Nilius, Efficient proximity effect correction method based on multivariate adaptive regression splines for grayscale e-beam lithography, J. Vac. Sci. Technol. B 32 (2014) 031602.
[21] C. Kaspar, J. Butschke, M. Irmscher, S. Martens, J.N. Burghartz, A new approach to determine development model parameters by employing the isotropy of the development process, Microelectron. Eng. 176 (2017) 79–83.
[22] C. Kaspar, J. Butschke, M. Irmscher, S. Martens, H. Sailer, R. Kirchner, V.A. Guzenko, H. Schift, J.N. Burghartz, Adjustable sidewall slopes by electron-beam exposure layout, J. Vac. Sci. Technol. B 35 (2017) 06G501.
[23] D. Daly, R.F. Stevens, M.C. Hutley, N. Davies, The manufacture of microlenses by melting photoresist, Meas. Sci. Technol. 1 (1990) 759–766.
[24] P. Ehbets, H.P. Herzig, D. Prongué, M.T. Gale, High-efficiency continuous surface-relief gratings for two-dimensional array generation, Opt. Lett. 17 (1992) 908–910 (1992).
[25] M.T. Gale, M. Rossi, H. Schütz, P. Ehbets, H.P. Herzig, D. Prongué, Continuous-relief diffractive optical elements for two-dimensional array generation, Appl. Opt. 32 (1993) 2526–2533.
[26] W. Däschner, P. Long, R. Stein, C. Wu, S.H. Lee, Cost-effective mass fabrication of multilevel diffractive optical elements by use of a single optical exposure with a gray-scale mask on high-energy beam-sensitive glass, Appl. Opt. 36 (1997) 4675–4680.
[27] C. Gimkiewicz, D. Hagedorn, J. Jahns, E.-B. Kley, F. Thoma, Fabrication of microprisms for planar optical interconnections by use of analog gray-scale lithography with high-energy-beam–sensitive glass, Appl. Opt. 38 (1999) 2986–2990.
[28] K. Reimer, U. Hofmann, M. Juerss, W. Pilz, H.J. Quenzer, B. Wagner, Fabrication of microrelief surfaces using a one-step lithography process, Proc. SPIE 3226 (1997).
[29] H.-C. Scheer, M. Wissen, N. Bogdanski, S. Möllenbeck, A. Mayer, Potential and limitations of a T-NIL/UVL hybrid process, Mircoelectron. Eng. 87 (2010) 851–853.
[30] C. Steinberg, M. Papenheim, S. Wang, H.-C. Scheer, Complex 3D structures via hybrid processing of SU-8, Microelectron. Eng. 155 (2016) 14–18.
[31] C.C. Han, J.C. Corelli, J.F. McDonald, Photosensitive UV resist of poly(methyl methacrylate) containing a bisazide compound, Nucl. Instrum. Methods Phys. Res. B 32 (1988) 422–426.
[32] D.J. Carbaugh, J.T. Wright, R. Parthiban, F. Rahman, Photolithography with polymethyl methacrylate (PMMA), Semicond. Sci. Technol. 31 (2016) 025010 (10 pp).
[33] R. Fallica, R. Kirchner, H. Schift, Y. Ekinci, High-Resolution Grayscale Patterning using Extreme Ultraviolet Interference Lithography, Microelectron. Eng. 177 (2017) 1–5.
[34] A. Schleunitz, C. Spreu, M. Vogler, H. Atasoy, H. Schift, Combining nanoimprint lithography and a molecular weight selective thermal reflow for the generation of mixed 3D structures, J. Vac. Sci. Technol. B 29 (2011) 06FC01 (4 pp).
[35] A. Schleunitz, V.A. Guzenko, A. Schander, M. Vogler, H. Schift, Selective profile transformation of electron-beam exposed multilevel resist structures based on a molecular weight dependent thermal reflow, J. Vac. Sci. Technol. B 29 (2011) 06F302 (4 pp).
[36] A. Schleunitz, V.A. Guzenko, M. Messerschmidt, H. Atasoy, R. Kirchner, H. Schift, Novel 3D micro- and nanofabrication method using thermally activated selective topography equilibration (TASTE) of polymers, Nano Converg. 1 (7) (2014) 1–8.
[37] C.-Y.- Chao, L.J. Guo, Reduction of surface scattering loss in polymer microrings using thermal-reflow technique, IEEE Photon. Technol. Let. 16 (2004) 1498–1500.
[38] Q. Xia, P.F. Murphy, H. Gao, S.Y. Chou, Ultrafast and selective reduction of sidewall roughness in silicon waveguides using self-perfection by liquefaction, Nanotechnology 20 (2009) 345302.
[39] A. Tulek, D. Akbulut, M. Bayindir, Ultralow threshold laser action from toroidal polymer microcavity, Appl. Phys. Lett. 94 (2009) 203302.
[40] K.A. Knapper, K.D. Heylman, E.H. Horak, R.H. Goldsmith, Chip-scale fabrication of high-Q all-glass toroidal microresonators for single-particle label-free imaging, Adv. Mater. 28 (2016) 2945–2950.
[41] D.E. Bornside, R.A. Brown, Global planarization of spun-on thin films by reflow, Appl. Phys. Lett. 58 (1991) 1181.
[42] E. Pargon, L. Azarnouche, M. Fouchier, K. Menguelti, J. Jussot, Smoothing mechanisms involved in thermal treatment for linewidth roughness reduction of 193-nm photoresist patterns, J. Vac. Sci. Technol. B 31 (2013) 061203.
[43] S.Y. Chou, L. Zhuang, Lithographically induced self-assembly of periodic polymer micropillar arrays, J. Vac. Sci. Technol. B 17 (1999) 3197–3202.
[44] S.Y. Chou, Nanoimprint lithography and lithographically induced self-assembly, MRS Bul. 26 (2001) 512–517.
[45] J.N.L. Albert, T.H. Epps III, Self-assembly of block copolymer thin films, Mater. Today 13 (2010) 24–33.
[46] K. Fuchs, C. Friedrich, J. Weese, Viscoelastic properties of narrow-distribution poly(methyl methacrylates), Macromolecules 29 (1996) 5893–5901.
[47] E.A. Dobisz, S.L. Brandow, R. Bass, J. Mitterender, Effects of molecular properties on nanolithography in polymethyl methacrylate, J. Vac. Sci. Technol. B 18 (2000) 107–111.
[48] G.S. Oehrlein, R.J. Phaneuf, D.B. Graves, Plasma-polymer interactions: a review of progress in understanding polymer resist mask durability during plasma etching for nanoscale fabrication, J. Vac. Sci. Technol. B 29 (2011) 010801 (35 pp).
[49] J.O. Choi, J.A. Moore, J.C. Corelli, J.P. Silverman, H. Bakhru, Degradation of poly (methylmethacrylate) by deep ultraviolet, x-ray, electron beam, and proton beam irradiations, J. Vac. Sci. Technol. B 6 (1988) 2286–2289.
[50] R. Fallica, J.K. Stowers, A. Grenville, A. Fromhold, A.P.G. Robinson, Dynamic absorption coefficients of CAR and non-CAR resists at EUV, Proc. SPIE 9776 (2016) 977612 (10 pp).
[51] S.-J. Li, S.-J. Xie, Y.-C. Li, H.-J. Qian, Z.-Y. Lu, Influence of molecular-weight polydispersity on the glass transition of polymers, Phys. Rev. E 93 (2016) 012613.
[52] R. Kirchner, N. Chidambaram, H. Schift, Benchmarking surface selective vacuum ultraviolet and thermal postprocessing of thermoplastics for ultrasmooth 3-D-printed micro-optics, Opt. Eng. 57 (2018) 041403 (11 pp).
[53] M. Ryu, D. Linklater, W. Hart, A. Balčytis, E. Skliutas, M. Malinauskas, D. Appadoo, Y.-R.E. Tan, E.P. Ivanova, J. Morikawa, S. Juodkazis, 3D printed polarizing grids for IR-THz synchrotron radiation, J. Opt. 20 (2018) 035101.
[54] S. Audran, B. Faure, B. Mortini, J. Regolini, G. Schlatter, G. Hadziioannou, Study of mechanisms involved in photoresist microlens formation, Microelectron. Eng. 83 (2006) 1087–1090.
[55] S. Audran, B. Mortini, B. Faure, G. Schlatter, Dynamical formation of microlenses by the reflow method: numerical simulation and experimental study of the process fabrication, J. Micromech. Microeng. 20 (2010) 095008 (9pp).
[56] MicroChemicals GmbH, Technical Information, Reflow of Photoresist (revised: Revised 1-11-2013) 〈https://www.microchemicals.com/technical_information/reflow_photoresist.pdf〉.
[57] D. Daly, R.F. Stevens, M.C. Hutley, N. Davies, The manufacture of microlenses by melting photoresist, Meas. Sci. Technol. 1 (1990) 759–766.
[58] H. Schift, Nanoimprint lithography: an old story in modern times? A review, J. Vac. Sci. Technol. B 26 (2008) 458–480.
[59] A. Franck, Kunststoff-Kompendium (Vogel Buchverlag, Würzburg, Auflage 4, 1996, p. 255.
[60] S. Abe, J.T. Sheridan, Curvature correction model of droplet profiles, Phys. Lett. A

253 (1999) 317–321.
[61] F.T. O'Neill, C.R. Walsh, J.T. Sheridan, Photoresist reflow method of microlens production: modeling and fabrication techniques, Proc. SPIE 5456 (2004) 197–208.
[62] T. Leveder, S. Landis, Reflow dynamics of thin patterned viscous films, Appl. Phys. Lett. 92 (2008) 013107.
[63] T. Leveder, E. Rognin, S. Landis, L. Davoust, Reflow of supported sub-100 nm polymer films as a characterization process for nanoimprint lithography, Microelectron. Eng. 88 (2011) 1867–1870.
[64] R. Kirchner, A. Schleunitz, H. Schift, Energy-based thermal reflow simulation for 3D polymer shape prediction using surface evolver, J. Micromech. Microeng. 24 (2014) 055010 (7pp).
[65] R. Kirchner, H. Schift, Mobility based 3D simulation of selective, viscoelastic polymer reflow using surface evolver, J. Vac. Sci. Technol. B 32 (2014) 06F701 (7pp).
[66] K.A. Brakke, The surface evolver, Exp. Math. 1 (1992) 141–165.
[67] Y.-Y. Chou, H.-J. Chang, J.-H. Kuo, W.-S. Hwang, The simulation of shape evolution of solder joints during reflow process and its experimental validation, Mater. Trans. 47 (2006) 1186–1192.
[68] J. Berthier, K.A. Brakke, The Physics of Microdroplets, Scrivener Publishing, Wiley, 2012.
[69] J. Berthier, K. Brakke, F. Grossi, L. Sanchez, L. Di Cioccio, Self-alignment of silicon chips on wafers: a capillary approach, J. Appl. Phys. 108 (2010) 054905 (10 pp).
[70] H. Teyssèdre, P. Gilormini, Extension of the natural element method to surface tension and wettability for the simulation of polymer flows at the micro and nano scales, J. Non-New. Fluid. Mech. 200 (2013) 9–16.
[71] H. Schift, C. Spreu, A. Schleunitz, J.J. Lee, Shape control of polymer reflow structures fabricated by nanoimprint lithography, Microelectron. Eng. 88 (2011) 87–92.
[72] J.M. Liu, Simple technique for measurements of pulsed Gaussian-beam spot sizes, Opt. Lett. 7 (1982) 196–198.
[73] J. Chalupský, L. Juha, J. Kuba, J. Cihelka, V. Hájková, S. Koptyaev, J. Krása, A. Velyhan, M. Bergh, C. Caleman, J. Hajdu, R.M. Bionta, H. Chapman, S.P. Hau-Riege, R.A. London, M. Jurek, J. Krzywinski, R. Nietubyc, J.B. Pelka, R. Sobierajski, J. Meyer-Ter-Vehn, A. Tronnier, K. Sokolowski-Tinten, N. Stojanovic, K. Tiedtke, S. Toleikis, T. Tschentscher, H. Wabnitz, U. Zastrau, Characteristics of focused soft X-ray free electron laser beam determined by ablation of organic molecular solids, Opt. Express 15 (2007) 6036–6043.
[74] J. Chalupský, J. Krzywinski, L. Juha, V. Hájková, J. Cihelka, T. Burian, L. Vysín, J. Gaudin, A. Gleeson, M. Jurek, A.R. Khorsand, D. Klinger, H. Wabnitz, R. Sobierajski, M. Störmer, K. Tiedtke, S. Toleikis, Spot size characterization of focused non-Gaussian X-ray laser beams, Opt. Express 18 (2010) 27836–27845.
[75] B. Rösner, F. Döring, P.R. Ribič, D. Gauthier, E. Principi, C. Masciovecchio, M. Zangrando, J. Vila-Comamala, G. de Ninno, C. David, High resolution beam profiling of X-ray free electron laser radiation by polymer imprint development, Opt. Express 25 (2017) 30686.
[76] P.F. Green, T.P. Russell, R. Jérôme, M. Granville, Diffusion of homopolymers into nonequilibrium block copolymer structures. 1. Molecular weight dependence, Macromolecules 21 (1988) 3266–3273.
[77] R. Kirchner, R. Hoekstra, N. Chidambaram, H. Schift, Depth-profiling of vertical material contrast after VUV exposure for contact-free polishing of 3D polymer micro-optics, Proc. SPIE 10446 (2017) 1044613 (9 pp).
[78] T. Hessler, M. Rossi, R.E. Kunz, M.T. Gale, Analysis and optimization of continuous-relief diffractive optical elements, Appl. Opt. 37 (1998) 4069–4079.
[79] D.C. O'Shea, T.J. Suleski, A.D. Kathman, D.W. Prather, Diffractive Optics, Design, Fabrication, and Test, Tutorial Texts in Optical Engineering, TT62 SPIE, 2004.
[80] M.A. Mohammad, M. Muhammad, S.K. Dew, M. Stepanova, Fundamentals of electron beam exposure and development, in: M. Stepanova, S.K. Dew (Eds.), Nanofabrication, Springer, 2012, pp. 11–41.
[81] M. Stepanova, T. Fito, Zs Szabóo, K. Alti, A.P. Adeyenuwo, K. Koshelev, M. Aktary, S.K. Dew, Simulation of electron beam lithography of nanostructures, J. Vac. Sci. Technol. B 28 (2010) C6C48.
[82] L.E. Ocola, A. Stein, Effect of cold development on improvement in electron-beam nanopatterning resolution and line roughness, J. Vac. Sci. Technol. B 24 (2006) 3061–3065.
[83] M. Otani, H. Asada, H. Tsunoda, M. Kunitake, T. Ishizaki, R. Miyagawa, Proc. SPIE 8081 (2011) 808107 (8 pp.).
[84] M. Schirmer, B. Büttner, F. Syrowatka, G. Schmidt, T. Köpnick, C. Kaiser, Proc. SPIE 8886 (2013) 88860D (7 pp.).
[85] S. Thoms, D.S. Macintyre, J. Vac. Sci. Technol. B 32 (2014) 06FJ01 (7 pp.).
[86] S. Pfirrmann, O. Lohse, V. Guzenko, A. Voigt, Towards a novel positive tone resist mr-PosEBR for high resolution electron-beam lithography, Microelectron. Eng. 155 (2016) 67–73.
[87] M.A. Mohammad, S.K. Dew, M. Stepanova, Nanoscale Res. Lett. 8 (2013) 139 (7 pp.).
[88] A. Gangnaik, Y.M. Georgiev, B. McCarthy, N. Petkov, V. Djara, J.D. Holmes, Microelectron. Eng. 123 (2014) 126–130.
[89] S. Pfirrmann, A. Voigt, A. Kolander, G. Grützner, O. Lohse, I. Harder, V.A. Guzenko, Towards a novel positive tone resist mr-PosEBR for high resolution electron-beam lithography, Microelectron. Eng. 155 (2016) 67–73.
[90] S. Pfirrmann, R. Kirchner, O. Lohse, V.A. Guzenko, A. Voigt, I. Harder, A. Kolander, H. Schift, G. Grützner, mr-PosEBR – a novel positive tone resist for high resolution electron beam lithography and 3D surface patterning, Proc. SPIE 9779 (2016) 977925 (13 pp).
[91] K. Nygard, S.P. Delcambre, D.K. Satapathy, O. Bunk, P.F. Nealey, F. van der Veen, Size-dependent shape evolution of patterned polymer films studied in situ by phase-retrieval-based small-angle X-ray scattering, Macromolecules 45 (2012) 5798–5805.
[92] N. Chidambaram, R. Kirchner, M. Altana, H. Schift, High fidelity 3D thermal nanoimprint with UV curable polydimethyl siloxane stamps, J. Vac. Sci. Technol. B 34 (2016) 06K401 (6 pp).
[93] H. Schift, Nanoimprint lithography: 2D or not 2D? A review, Appl. Phys. A 121 (2015) 415–435.
[94] R. Kirchner, V.A. Guzenko, M. Rohn, E. Sonntag, M. Mühlberger, I. Bergmair, H. Schift, Bio-inspired 3D funnel structures made by grayscale electron-beam patterning and selective topography equilibration, Microelectron. Eng. 141 (2015) 107–111.
[95] M. Mühlberger, M. Rohn, J. Danzberger, E. Sonntag, A. Rank, L. Schumm, R. Kirchner, C. Forsich, S. Gorb, B. Einwögerer, E. Trapple, D. Heim, H. Schift, I. Bergmair, UV-NIL fabricated bio-inspired inlays for injection molding to influence the friction behavior of ceramic surfaces, Microelectron. Eng. 141 (2015) 140–144.
[96] R.R.A. Syms, E.M. Yeatman, Self-assembly of three-dimensional microstructures using rotation by surface tension forces, Electron. Lett. 29 (1993) 662–664.
[97] R.A. Syms, Surface tension powered self-assembly of 3-D micro-optomechanical structures, J. MEMS 8 (1999) 448–455.
[98] J.-H. Cho, D. Gracias, Self-assembly of lithographically patterned nanoparticles, Nano Let. 9 (2009) 4049–4052.
[99] Y.K. Hong, R.A.A. Syms, Stability of surface tension self-assembled 3D MOEMS, Sens. Actuators A 127 (2006) 381–391.
[100] J.-H. Cho, A. Azam, D.H. Gracias, ThreE Dimensional Nanofabrication Using Surface Forces, Langmuir 26 (2010) 16534–16539.
[101] A. Azam, K.E. Lafli, M. Jamal, R. Fernandes, D.H. Gracias, Self-folding micropatterned polymeric containers, Biomed. Microdev. 13 (2011) 51–58.
[102] R. Fernandes, D.H. Gracias, Self-folding polymeric containers for encapsulation and delivery of drugs, Adv. Drug Deliv. Rev. 64 (2012) 1579–1589.
[103] B. Chang, Q. Zhou, Z. Wu, Z. Liu, R.H.A. Ras, K. Hjort, Capillary self-alignment of microchips on soft substrates, Micromachines 7 (41) (2016) (9 pp.).